INFLUENCE OF AN ASYMMETRIC RING ON THE MODELING OF AN ORTHOGONALLY STIFFENED CYLINDRICAL SHELL

Naveen Rastogi* and Eric R. Johnson†

Virginia Polytechnic Institute and State University

Blacksburg, Virginia 24061

ABSTRACT

Structural models are examined for the influence of a ring with an asymmetrical cross section on the linear elastic response of an orthogonally stiffened cylindrical shell subjected to internal pressure. The first structural model employs classical theory for the shell and stiffeners. The second model employs transverse shear deformation theories for the shell and stringer, and classical theory for the ring. Closed-end pressure vessel effects are included. Interacting line load intensities are computed in the stiffener-to-skin joints for an example problem having the dimensions of the fuselage of a large transport aircraft. Classical structural theory is found to exaggerate the asymmetric response compared to the transverse shear deformation theory.

INTRODUCTION

The cabin pressurization in a transport aircraft causes about a 10 psi pressure differential across the skin. An unstiffened, or a monocoque fuselage would carry this internal pressure load as a shell in membrane response, like a pressure vessel. However, internal longitudinal and transverse stiffeners are necessary to carry loads due to flight maneuvers, landing and ground handling, etc. How the loads are transferred in the stiffener-to-skin joints under pressurization is necessary for determining the load capacity of these joints.

---

* Graduate Research Assistant, Aerospace and Ocean Engineering

† Professor of Aerospace and Ocean Engineering

The design of stiffener-to-skin joints was cited by Jackson, et al. (1984) as one of the major technology issues in utilizing graphite/epoxy composites in the fuselage of a large transport aircraft. Stiffeners can be attached to the skin by either fasteners, co-curing, adhesive bonding, or some combination of these methods. Where fasteners are required in a graphite/epoxy structure, aluminium fasteners cannot be used because of galvanic corrosion to the metal. More expensive fasteners, like titanium, are required to avoid corrosion.

A ring, or frame, with asymmetrical cross section is commonly used as a transverse stiffening member in the fuselage of a transport aircraft. The influence of this ring asymmetry on the distribution of the interacting loads in the stiffener-to-skin joint is the subject of this paper. Two structural models are considered. The first model employs classical theory for the shell and the stiffeners. The second model employs transverse shear deformation theories for the shell and stringer, and classical theory for the ring. We have previously published results for the response with symmetrical section rings and stringers using classical theory (Johnson and Rastogi, 1994).

Hence, the objective of this paper is to examine structural models for the linear elastic response of an orthogonally stiffened, composite material cylindrical shell subjected to internal pressure, where the ring has an asymmetrical cross section and the stringer has a symmetrical cross section. This objective is part of a larger effort to develop an analysis/design capability for the stiffener-to-skin joint of a large transport aircraft. A potential benefit of such an analysis/design capability is to use fewer expensive fasteners in the graphite/epoxy fuselage.

MATHEMATICAL MODEL

An idealized mathematical model is assumed for the semi-monocoque fuselage to study the generic characteristics of the response in the vicinity of the stiffeners' intersection. The model is of a very long circular cylindrical shell internally stiffened by identical stringers equally spaced around the circumference, and identical frames

or rings, equally spaced along the length. In general, the spacing of the stringers is not the same as that of the rings. The structure is periodic both longitudinally and circumferentially, and the loading is spatially uniform. Consequently, a structural repeating unit can be defined whose deformation determines the deformation of the entire structure. A typical repeating unit consists of a portion of the shell wall centered over the portions of stringer and ring as shown in Fig. 1. The radius of the middle surface of the undeformed cylindrical shell is denoted by R, and the thickness of the shell is denoted by t. Axial coordinate x and the circumferential angle θ are lines of curvature on the middle surface, and the thickness coordinate is denoted by z, with $-t/2 \leq z \leq t/2$. The origin of the surface coordinates is centered over the stiffeners intersection so that $-l \leq x \leq l$ and $-\Theta \leq \theta \leq \Theta$, where $2l$ is the axial length, and $2R\Theta$ is the circumferential arc length of the repeating unit.

The stiffeners are mathematically modeled as one-dimensional elements, or discrete beams, so that the actions transmitted by the stiffeners to the inside of the shell wall are represented by distributed line load intensities. In this paper it is assumed that the stringer is symmetric about the x-z plane through its centroidal axis and the ring is asymmetric. On the basis of the symmetry about the x-axis for the unit, only the interacting line load components tangent and normal to the stringer are included in the analysis. However, due to an asymmetric ring, the interacting line loads between shell and the ring consist of three distributed force components and a tangential distributed moment component. The shell-stringer interacting force components per unit length along the contact lines are denoted by $\lambda_{xs}(x)$ for the component tangent to the stringer and $\lambda_{zs}(x)$ for the component normal to the stringer. The three shell-ring interacting force components per unit length along the contact lines are denoted by $\lambda_{xr}(\theta)$ for the component acting in the axial direction, $\lambda_{\theta r}(\theta)$ for the component tangent to the ring, and $\lambda_{zr}(\theta)$ for the component normal to the ring. The shell-ring interacting moment component, tangent to the ring, per unit length along the contact line is denoted by $\Lambda_{\theta r}(\theta)$.

These interacting loads acting in a positive sense on the inside surface of the shell are shown in Fig. 2. The purpose of the analysis is to determine these distributed line load intensities and also, to examine the differences in their distribution for the two structural models described earlier.

For both models, the linear elastic response of the repeating unit to internal pressure is obtained by utilizing Ritz method and the principle of virtual work applied separately to the shell, stringer, and ring. The virtual work functionals are augmented by Lagrange multipliers to enforce kinematic constraints between the structural components of the repeating unit. The Lagrange multipliers represent the interacting line loads between the stiffeners and the shell. Displacements are separately assumed for the shell, stringer, and the ring.

TRANSVERSE SHEAR DEFORMATION FORMULATIONS

Shell

A consistent first order transverse shear deformation theory is developed to model the shell. Based on the assumption that the shell thickness t is relatively small and hence, does not change during loading, the displacements at an arbitrary material point in the shell are approximated by

$$U(x,\theta,z) = u(x,\theta) + z\phi_x(x,\theta) \tag{1}$$

$$V(x,\theta,z) = v(x,\theta) + z\phi_\theta(x,\theta) \tag{2}$$

$$W(x,\theta,z) = w(x,\theta) \tag{3}$$

where $u(x,\theta)$, $v(x,\theta)$ and $w(x,\theta)$ are the displacements of the points of the reference surface, and $\phi_x(x,\theta)$ and $\phi_\theta(x,\theta)$ are the rotations of the normal to the reference surface as shown in Fig. 3(a). Using Eqs. (1) to (3) and assuming small displacement gradients, the three-dimensional engineering strains are

$$e_{xx} = \epsilon_{xx} + z\kappa_{xx} \qquad e_{\theta\theta} = \frac{\epsilon_{\theta\theta} + z\kappa_{\theta\theta}}{(1+\frac{z}{R})} \qquad e_{zz} = 0 \tag{4}$$

$$e_{x\theta} = \frac{\gamma_{x\theta} + z(1+\frac{z}{2R})\bar{\kappa}_{x\theta} + \frac{z^2}{2R}\tilde{\kappa}_{x\theta}}{(1+\frac{z}{R})} \tag{5}$$

$$e_{xz} = \gamma_{xz} \qquad e_{\theta z} = \frac{\gamma_{\theta z}}{(1+\frac{z}{R})} \tag{6}$$

The transverse shear strains e_{xz} and $e_{\theta z}$ represent average transverse shearing strains through the thickness of the shell since Eqs. (1) to (3) are approximate in the z-coordinate. In Eqs. (4) to (6), the two-dimensional, or shell, strain measures, which are independent of the z-coordinate, are defined by

$$\epsilon_{xx} = \frac{\partial u}{\partial x} \qquad \kappa_{xx} = \frac{\partial \phi_x}{\partial x} \tag{7}$$

$$\epsilon_{\theta\theta} = \frac{1}{R}\frac{\partial v}{\partial \theta} + \frac{w}{R} \qquad \kappa_{\theta\theta} = \frac{1}{R}\frac{\partial \phi_\theta}{\partial \theta} \tag{8}$$

$$\gamma_{x\theta} = \frac{\partial v}{\partial x} + \frac{1}{R}\frac{\partial u}{\partial \theta} \tag{9}$$

$$\bar{\kappa}_{x\theta} = \frac{\partial \phi_\theta}{\partial x} + \frac{1}{R}\frac{\partial \phi_x}{\partial \theta} + \frac{1}{R}\frac{\partial v}{\partial x} \tag{10}$$

$$\tilde{\kappa}_{x\theta} = \frac{\partial \phi_\theta}{\partial x} - \frac{1}{R}\frac{\partial \phi_x}{\partial \theta} - \frac{1}{R}\frac{\partial v}{\partial x} \tag{11}$$

$$\gamma_{xz} = \phi_x + \frac{\partial w}{\partial x} \qquad \gamma_{\theta z} = \phi_\theta - \frac{v}{R} + \frac{1}{R}\frac{\partial w}{\partial \theta} \tag{12}$$

If we set the (average) transverse shear strains in Eq. (6) to zero, then the rotations of the normal are

$$\phi_x = -\frac{\partial w}{\partial x} \tag{13}$$

$$\phi_\theta = \frac{v}{R} - \frac{1}{R}\frac{\partial w}{\partial \theta} \tag{14}$$

so that

$$\kappa_{x\theta} = \bar{\kappa}_{x\theta} = -\frac{2}{R}\frac{\partial^2 w}{\partial x \partial \theta} + \frac{2}{R}\frac{\partial v}{\partial x} \qquad \tilde{\kappa}_{x\theta} = 0 \tag{15}$$

Hence, the thickness distribution of the shear strain reduces to

$$e_{x\theta} = \frac{\gamma_{x\theta} + z(1+\frac{z}{2R})\kappa_{x\theta}}{(1+\frac{z}{R})} \tag{16}$$

which coincides with the results of Novozhilov's (1964) classical shell theory.

It is evident from Eq. (5) that three shell strain measures are needed to represent the shear strain distribution through the thickness in the transverse shear deformation shell theory. Whereas, only two shell strain measures are required in classical shell theory to represent the shearing strain distribution through the thickness (refer to Eq. (16)). Also it can be shown that under rigid body rotation of the shell, the nine shell strain measures, given by Eqs. (7) through (12) vanish. (For Novozhilov's classical shell theory, six shell strain measures given by Eqs. (7-9) and (15) vanish under rigid body rotations).

The physical shell stress resultants and stress couples in terms of stress components are given, in usual way, by

$$\begin{aligned}
(N_{xx},\ M_{xx}) &= \int_t (1, z)\sigma_{xx}(1 + \frac{z}{R})\ dz \\
(N_{\theta\theta},\ M_{\theta\theta}) &= \int_t (1, z)\sigma_{\theta\theta}\ dz \\
(N_{x\theta},\ M_{x\theta}) &= \int_t (1, z)\sigma_{x\theta}(1 + \frac{z}{R})\ dz \\
(N_{\theta x},\ M_{\theta x}) &= \int_t (1, z)\sigma_{\theta x}\ dz \\
Q_x &= \int_t \sigma_{xz}(1 + \frac{z}{R})\ dz \\
Q_\theta &= \int_t \sigma_{\theta z} dz
\end{aligned} \tag{17}$$

A generalized 9×1 stress vector for the shell is defined by

$$\vec{\sigma}_{shell} = [N_{xx}, N_{\theta\theta}, N_{\theta x}, M_{xx}, M_{\theta\theta}, \bar{M}_{x\theta}, \tilde{M}_{x\theta}, Q_x, Q_\theta]^T \tag{18}$$

in which $\bar{M}_{x\theta}$ and $\tilde{M}_{x\theta}$ are the mathematical quantities conjugate to the modified twisting measures $\bar{\kappa}_{x\theta}$ and $\tilde{\kappa}_{x\theta}$, respectively, and are defined in terms of the physical stress couples by

$$\bar{M}_{x\theta} = \frac{1}{2}(M_{x\theta} + M_{\theta x}) \qquad \tilde{M}_{x\theta} = \frac{1}{2}(M_{x\theta} - M_{\theta x}) \tag{19}$$

The nine elements of the stress vector in Eq. (18) and the relations of Eq. (19) determine all the stress resultants and stress couples listed in Eq. (17) except for shear resultant $N_{x\theta}$. The shear stress resultant $N_{x\theta}$ is determined from moment equilibrium about the normal for an element of the shell. This so-called sixth equilibrium equation is

$$N_{x\theta} = N_{\theta x} + \frac{M_{\theta x}}{R} \tag{20}$$

The generalized strain vector for the shell is

$$\vec{\epsilon}_{shell} = [\epsilon_{xx}, \epsilon_{\theta\theta}, \gamma_{x\theta}, \kappa_{xx}, \kappa_{\theta\theta}, \bar{\kappa}_{x\theta}, \tilde{\kappa}_{x\theta}, \gamma_{xz}, \gamma_{\theta z}]^T \tag{21}$$

This strain vector is conjugate to the stress vector in the sense that the internal virtual work for the shell is given by

$$\delta \mathcal{W}^{int}_{shell} = \iint_S \delta \vec{\epsilon}^T_{shell}\ \vec{\sigma}_{shell}\ dS \tag{22}$$

where S denotes the area of the reference surface and $dS = dxRd\theta$. This expression for the internal virtual work can be derived from three-dimensional elasticity theory by using Eqs. (4) to (6) for the thickness distributions of the strains and the definitions of the resultants given by Eqs. (17) and (19).

Consistent with the transverse shear deformation theory, the linear elastic constitutive law for a laminated composite shell wall is given by

$$\begin{Bmatrix} N_{xx} \\ N_{\theta\theta} \\ N_{\theta x} \\ M_{xx} \\ M_{\theta\theta} \\ \bar{M}_{x\theta} \\ \tilde{M}_{x\theta} \end{Bmatrix} = \begin{bmatrix} A_{11} & A_{12} & A_{16} & B_{11} & B_{12} & B^1_{16} & B^2_{16} \\ A_{12} & A_{22} & A_{26} & B_{12} & B_{22} & B^1_{26} & B^2_{26} \\ A_{16} & A_{26} & A_{66} & B_{61} & B_{62} & B^1_{66} & B^2_{66} \\ B_{11} & B_{12} & B_{61} & D_{11} & D_{12} & D^1_{16} & D^2_{16} \\ B_{12} & B_{22} & B_{62} & D_{12} & D_{22} & D^1_{26} & D^2_{26} \\ B^1_{16} & B^1_{26} & B^1_{66} & D^1_{16} & D^1_{26} & D^{11}_{66} & D^{12}_{66} \\ B^2_{16} & B^2_{26} & B^2_{66} & D^2_{16} & D^2_{26} & D^{12}_{66} & D^{22}_{66} \end{bmatrix} \begin{Bmatrix} \epsilon_{xx} \\ \epsilon_{\theta\theta} \\ \gamma_{x\theta} \\ \kappa_{xx} \\ \kappa_{\theta\theta} \\ \bar{\kappa}_{x\theta} \\ \tilde{\kappa}_{x\theta} \end{Bmatrix} \tag{23}$$

and

$$\begin{Bmatrix} Q_x \\ Q_\theta \end{Bmatrix} = \begin{bmatrix} A_{44} & A_{45} \\ A_{45} & A_{55} \end{bmatrix} \begin{Bmatrix} \gamma_{xz} \\ \gamma_{\theta z} \end{Bmatrix} \tag{24}$$

in which stiffnesses A_{ij}, B_{ij} and D_{ij} are given in Appendix. The transverse shear stiffnesses, A_{44}, A_{45}, and A_{55} can be calculated by two different methods. The first method is based on the assumption of constant transverse shear strain distribution through the thickness, and the second method is based on the assumption of constant transverse shear stress distribution through the thickness. In the present analysis, we have used the first method to compute the transverse shear stiffnesses.

The statement of virtual work is

$$\delta W^{int}_{shell} = \delta W^{ext}_{p} + \delta W^{ext}_{\lambda} \tag{25}$$

where the external virtual work for a cylindrical shell under constant internal pressure, including an axial load due to the closed-end effect, is written as

$$\delta W^{ext}_{p} = \iint_{S} p\ \delta w\ dS \quad + \quad p \int_{-\Theta}^{\Theta} \frac{R^2}{2} d\theta\ [\delta u(l,\theta) - \delta u(-l,\theta)] \tag{26}$$

and the external (or augmented) virtual work due to the interacting loads is

$$\begin{aligned}
\delta W^{ext}_{\lambda} = & \int_{-l}^{l} \Big\{ \lambda_{xs}(x)\big[\delta u(x,0) - \frac{t}{2}\delta\phi_x(x,0)\big] + \lambda_{zs}(x)\delta w(x,0) \Big\}\ dx \\
& + \int_{-\Theta}^{\Theta} \Big\{ \lambda_{xr}(\theta)\big[\delta u(0,\theta) - \frac{t}{2}\delta\phi_x(0,\theta)\big] + \lambda_{\theta r}(\theta)\big[\delta v(0,\theta) - \frac{t}{2}\delta\phi_\theta(0,\theta)\big] \\
& + \lambda_{zr}(\theta)\delta w(0,\theta) - \Lambda_{\theta r}(\theta)\delta\big(\frac{\partial w}{\partial x}\big|_{x=0}\big) \Big\}\ (R - \frac{t}{2}) d\theta - Q[\delta u(l,0) - \delta u(-l,0)]
\end{aligned} \tag{27}$$

The axial force Q in Eq. (27) is an additional Lagrange multiplier that accounts for axial load sharing between the stringer and shell.

Stringer

Stringer displacements $u_s(x)$ and $w_s(x)$, and the rotation of the normal $\phi_{\theta s}(x)$ are shown in Fig. 3(b). Based on transverse shear deformation theory, the virtual

work expression for the stringer is

$$\int_{-l}^{l} [N_{xs}\delta\epsilon_{xs} + M_{\theta s}\delta\kappa_{\theta s} + V_s\delta\gamma_{zs}]dx = -\int_{-l}^{l} \Big\{\lambda_{xs}(x)[\delta u_s(x) + e_s\delta\phi_{\theta s}(x)] + \lambda_{zs}(x)\delta w_s(x)\Big\}\, dx + Q[\delta u_s(l) - \delta u_s(-l)] \tag{28}$$

in which N_{xs} is the axial force in the stringer, $M_{\theta s}$ is the bending moment, V_s is the transverse shear force, ϵ_{xs} is the normal strain of the centroidal line, the product $z\kappa_{\theta s}$ is the portion of the axial normal strain due to bending, γ_{zs} is the transverse shear strain, and e_s is the radial distance from the stringer centroid to the contact line along the shell inside surface. The strain-displacement relations and Hooke's law for the stringer are

$$\epsilon_{xs} = u'_s \qquad \kappa_{\theta s} = \phi'_{\theta s} \qquad \gamma_{zs} = \phi_{\theta s} + w'_s \tag{29}$$

$$N_{xs} = (EA)_s\epsilon_{xs} \qquad M_{\theta s} = (EI)_s\kappa_{\theta s} \qquad V_s = (GA)_s\gamma_{zs} \tag{30}$$

in which the prime denotes an ordinary derivative with respect to x.

CLASSICAL FORMULATIONS

Shell

The shell is modeled with Sanders' (1959) theory for thin shells. Define a generalized strain vector in terms of the shell strain measures by

$$\vec{\epsilon}_{shell} = [\epsilon_{xx}, \epsilon_{\theta\theta}, \gamma_{x\theta}, \kappa_{xx}, \kappa_{\theta\theta}, \kappa_{x\theta}]^T \tag{31}$$

The first five strain measures of the shell reference surface in Eq. (31) are related to the displacements by Eqs. (7-9), and the sixth strain measure, $\kappa_{x\theta}$, is given by

$$\kappa_{x\theta} = \frac{\partial\phi_\theta}{\partial x} + \frac{1}{R}\frac{\partial\phi_x}{\partial\theta} + \frac{1}{R}\phi \tag{32}$$

where the rotation about the normal, ϕ, is

$$\phi = \frac{1}{2}\left(\frac{\partial v}{\partial x} - \frac{1}{R}\frac{\partial u}{\partial\theta}\right) \tag{33}$$

and the rotations ϕ_x and ϕ_θ of the normal are given by Eqs. (13) and (14).

Define a generalized stress vector in terms of the stress resultants and couples of Sanders' theory by

$$\vec{\sigma}_{shell} = [N_{xx}, N_{\theta\theta}, N^s_{x\theta}, M_{xx}, M_{\theta\theta}, M^s_{x\theta}]^T \tag{34}$$

such that the internal virtual work is given by Eq. (22). Quantities $N^s_{x\theta}$ and $M^s_{x\theta}$ are the modified shear resultant and twisting moment resultant in the Sanders theory. Hooke's law for a laminated composite shell wall is

$$\vec{\sigma}_{shell} = H\vec{\epsilon}_{shell} \qquad H = \begin{bmatrix} A & B \\ B^T & D \end{bmatrix} \tag{35}$$

in which the 3×3 sub-matrices A, B and D are given by classical lamination theory (Jones, 1975). The external virtual work expressions for the classical shell theory are still given by Eqs. (26) and (27), but the rotations in Eqs. (27) are given by Eqs. (13) and (14).

Stringer

The stringer is modeled with Euler-Bernoulli beam theory thereby neglecting the transverse shear strain. Hence, equating γ_{zs} in Eq. (29) to zero results in the following expression for $\phi_{\theta s}$.

$$\phi_{\theta s} = -w'_s \tag{36}$$

It may be noted that neglecting the transverse shear strain would also modify the virtual work statement given by Eq. (28), and the third equation in the Hooke's law, Eq. (30), is neglected.

Ring

Ring displacements are denoted $u_r(\theta)$, $v_r(\theta)$, and $w_r(\theta)$, and the rotations are denoted by $\phi_{xr}(\theta)$, $\phi_{\theta r}(\theta)$, and $\phi_{zr}(\theta)$ as shown in Fig. 3(c). The structural model

is based on Euler-Bernoulli hypotheses. The statement of virtual work is

$$\int_{-\Theta}^{\Theta} [N_{\theta r}\delta\epsilon_{\theta r} + M_{xr}\delta\kappa_{xr} + M_{zr}\delta\kappa_{zr} + T_r\delta\tau_r]R_0\ d\theta =$$

$$-\int_{-\Theta}^{\Theta} \Big\{\lambda_{xr}(\theta)\big[\delta u_r(\theta) + e_r\delta\phi_{\theta r}(\theta)\big] + \lambda_{\theta r}(\theta)\big[\delta v_r(\theta) + e_r\delta\phi_{xr}(\theta)\big] \tag{37}$$

$$+ \lambda_{zr}(\theta)\delta w_r(\theta) + \Lambda_{\theta r}(\theta)\delta\phi_{\theta r}(\theta)\Big\}\ (1 + \frac{e_r}{R_0})\ R_0\ d\theta$$

in which $N_{\theta r}$ is the circumferential force, M_{xr} is the in-plane bending moment, M_{zr} is the out-of-plane bending moment, T_r is the torque, $\epsilon_{\theta r}$ is the circumferential normal strain of the centroidal arc, κ_{xr} is the change in curvature due to in-plane bending, κ_{zr} is the change in curvature due to out-of-plane bending, τ_r is the twist rate, e_r is the distance from the ring reference arc to the contact line along the shell inside surface, and R_0 is the radius of ring reference arc. The rotations and strain-displacement relations are

$$\begin{aligned}
&\epsilon_{\theta r} = \frac{1}{R_0}(\dot{v}_r + w_r) \qquad && \kappa_{xr} = \frac{1}{R_0}\dot{\phi}_{xr} \qquad && \kappa_{zr} = \frac{1}{R_0}(\dot{\phi}_{zr} - \phi_{\theta r}) \\
&\tau_r = \frac{1}{R_0}(\dot{\phi}_{\theta r} + \phi_{zr}) \qquad && \phi_{xr} = \frac{1}{R_0}(v_r - \dot{w}_r) \qquad && \phi_{zr} = -\frac{1}{R_0}\dot{u}_r
\end{aligned} \tag{38}$$

in which ϕ_{xr} is the rotation around x-axis, ϕ_{zr} is the rotation around z-axis, and the over-dot denotes an ordinary derivative with respect to θ. Hooke's law is

$$\begin{aligned}
&N_{\theta r} = (EA)_r\epsilon_{\theta r} \qquad && M_{xr} = (EI_{xx})_r\kappa_{xr} - (EI_{zx})_r\kappa_{zr} \\
&M_{zr} = (EI_{zz})_r\kappa_{zr} - (EI_{zx})_r\kappa_{xr} \qquad && T_r = (GJ)_r\tau_r
\end{aligned} \tag{39}$$

DISPLACEMENT CONTINUITY

In order to maintain continuous deformation between the inside surface of the shell and stiffeners along their lines of contact, the following displacement continuity constraints are imposed:

Along the shell - stringer interface (i.e., $-l \le x \le l$, $\theta = 0$),

$$g_{xs} = u(x,0) - \frac{t}{2}\phi_x(x,0) - \big[u_s(x) + e_s\phi_{\theta s}(x)\big] = 0 \tag{40}$$

$$g_{zs} = w(x,0) - w_s(x) = 0 \tag{41}$$

Along the shell - ring interface (i.e., $x = 0$, $-\Theta \leq \theta \leq \Theta$),

$$g_{xr} = u(0,\theta) - \frac{t}{2}\phi_x(0,\theta) - \left[u_r(\theta) + e_r\phi_{\theta r}(\theta)\right] = 0 \tag{42}$$

$$g_{\theta r} = v(0,\theta) - \frac{t}{2}\phi_\theta(0,\theta) - \left[v_r(\theta) + e_r\phi_{xr}(\theta)\right] = 0 \tag{43}$$

$$g_{zr} = w(0,\theta) - w_r(\theta) = 0 \tag{44}$$

$$G_{\theta r} = -\frac{\partial w}{\partial x}\Big|_{x=0} - \phi_{\theta r}(\theta) = 0 \tag{45}$$

The variational form of these constraints are

$$\int_{-l}^{l} \left[\delta\lambda_{xs}g_{xs} + \delta\lambda_{zs}g_{zs}\right]\, dx \;=\; 0 \tag{46}$$

$$\int_{-\Theta}^{\Theta} \left[\delta\lambda_{xr}g_{xr} + \delta\lambda_{\theta r}g_{\theta r} + \delta\lambda_{zr}g_{zr} + \delta\Lambda_{\theta r}G_{\theta r}\right]\, (R_0 + e_r)\, d\theta \;=\; 0 \tag{47}$$

The constraint that the elongation of the shell at $\theta = 0$ and the elongation of the stringer are the same is

$$\delta Q\left\{\left[u(l,0) - u(-l,0)\right] - \left[u_s(l) - u_s(-l)\right]\right\} \;=\; 0 \tag{48}$$

DISPLACEMENTS, ROTATIONS, AND INTERACTING LOAD APPROXIMATIONS

The periodic portions of the displacements and rotations are represented by truncated Fourier Series having fundamental periods in the stringer and ring spacing. The non-periodic portions of the displacements due to axial stretching are represented by simple terms in x. The Fourier series reflect symmetry about the x-axis for the repeating unit. For the shell, displacements of the middle surface (see Fig. 3a) are represented as

$$u(x,\theta) = \frac{q_0 x}{2l} + \sum_{m=1}^{M}\sum_{n=0}^{N} u_{1mn}Sin(\alpha_m x)Cos(\beta_n\theta) + \sum_{m=1}^{M}\sum_{n=1}^{N} u_{2mn}Cos(\alpha_m x)Cos(\beta_n\theta) \tag{49}$$

$$v(x,\theta) = \sum_{m=0}^{M}\sum_{n=1}^{N} v_{1mn}Cos(\alpha_m x)Sin(\beta_n\theta) + \sum_{m=1}^{M}\sum_{n=1}^{N} v_{2mn}Sin(\alpha_m x)Sin(\beta_n\theta) \quad (50)$$

$$w(x,\theta) = \sum_{m=0}^{M}\sum_{n=0}^{N} w_{1mn}Cos(\alpha_m x)Cos(\beta_n\theta) + \sum_{m=1}^{M}\sum_{n=1}^{N} w_{2mn}Sin(\alpha_m x)Cos(\beta_n\theta) \quad (51)$$

and rotations of the normal are

$$\phi_x(x,\theta) = \sum_{m=1}^{M}\sum_{n=0}^{N} \phi_{x1mn}Sin(\alpha_m x)Cos(\beta_n\theta) + \sum_{m=1}^{M}\sum_{n=1}^{N} \phi_{x2mn}Cos(\alpha_m x)Cos(\beta_n\theta) \quad (52)$$

$$\phi_\theta(x,\theta) = \sum_{m=0}^{M}\sum_{n=1}^{N} \phi_{\theta1mn}Cos(\alpha_m x)Sin(\beta_n\theta) + \sum_{m=1}^{M}\sum_{n=1}^{N} \phi_{\theta2mn}Sin(\alpha_m x)Sin(\beta_n\theta) \quad (53)$$

in which $\alpha_m = \frac{m\pi}{l}$ and $\beta_n = \frac{n\pi}{\Theta}$ where m and n are non-negative integers. Note that some terms in the truncated Fourier Series of Eqs. (49-53) have been omitted. The coefficients of the omitted terms are u_{200}, u_{2m0}, u_{20n}, w_{2m0}, ϕ_{x200}, ϕ_{x2m0}, and ϕ_{x20n}, in which $m = 1, 2, ..., M$ and $n = 1, 2, ..., N$. The rationale for their omission is discussed in the following sub-section. The displacements of the centroidal line of stringer (see Fig. 3b) are

$$u_s(x) = \frac{q_1 x}{2l} + \sum_{m=1}^{M} u_{s1m}Sin(\alpha_m x) + \sum_{m=1}^{M} u_{s2m}Cos(\alpha_m x) \quad (54)$$

$$w_s(x) = \sum_{m=1}^{M} w_{s1m}Sin(\alpha_m x) + \sum_{m=1}^{M} w_{s2m}Cos(\alpha_m x) \quad (55)$$

and the rotation of the normal of the stringer about the θ-axis is

$$\phi_{\theta s}(x) = \sum_{m=1}^{M} \phi_{\theta s1m}Sin(\alpha_m x) + \sum_{m=1}^{M} \phi_{\theta s2m}Cos(\alpha_m x) \quad (56)$$

where the coeffcients u_{s20} , w_{s20} and $\phi_{\theta s20}$ are omitted. Coefficient q_0 in the axial displacement field of the shell and q_1 in the axial displacement field of the stringer represent elongations of each respective element caused by either an axial mechanical

load or due to close-end pressure vessel effects. The displacements of the reference circle of the ring (see Fig. 3c) are

$$u_r(\theta) = \sum_{n=1}^{N} u_{rn} Cos(\beta_n \theta) \tag{57}$$

$$v_r(\theta) = \sum_{n=1}^{N} v_{rn} Sin(\beta_n \theta) \tag{58}$$

$$w_r(\theta) = \sum_{n=0}^{N} w_{rn} Cos(\beta_n \theta) \tag{59}$$

and twist of the ring is

$$\phi_{\theta r}(\theta) = \sum_{n=1}^{N} \phi_{\theta rn} Cos(\beta_n \theta) \tag{60}$$

where the coeffcients u_{r0} and $\phi_{\theta r0}$ are omitted. The distributions of the interacting loads, or Lagrange multipliers, are taken as

$$\lambda_{xs}(x) = \sum_{m=1}^{M} \lambda_{xs1m} Sin(\alpha_m x) + \sum_{m=1}^{M} \lambda_{xs2m} Cos(\alpha_m x) \tag{61}$$

$$\lambda_{zs}(x) = \sum_{m=1}^{M} \lambda_{zs1m} Sin(\alpha_m x) + \sum_{m=1}^{M} \lambda_{zs2m} Cos(\alpha_m x) \tag{62}$$

$$\lambda_{xr}(\theta) = \sum_{n=1}^{N} \lambda_{xrn} Cos(\beta_n \theta) \tag{63}$$

$$\lambda_{\theta r}(\theta) = \sum_{n=1}^{N} \lambda_{\theta rn} Sin(\beta_n \theta) \tag{64}$$

$$\lambda_{zr}(\theta) = \sum_{n=0}^{N} \lambda_{zrn} Cos(\beta_n \theta) \tag{65}$$

$$\Lambda_{\theta r}(\theta) = \sum_{n=1}^{N} \Lambda_{\theta rn} Cos(\beta_n \theta) \tag{66}$$

where the coefficients λ_{x2s0}, λ_{z2s0}, λ_{xr0}, and $\Lambda_{\theta r0}$ are omitted.

Terms Omitted in the Fourier Series

Terms omitted in the truncated Fourier Series for the displacements, rotations, and the interacting loads were determined from rigid body equilibrium conditions for the ring and stringer, and from displacement continuity conditions between the shell and the stiffeners. The external virtual work for the stringer and ring must vanish for any possible rigid body motions of these elements. For the stringer these rigid body motions are spatially uniform x-direction and z-direction displacements. (A rigid body rotation of the stringer in the x-z plane is not considered since this motion would violate longitudinal periodicity of the repeating units.) Vanishing of the external virtual work for an arbitrary rigid body displacement of the stringer in the axial direction leads to the x-direction equilibrium equation

$$\int_{-l}^{l} \lambda_{xs}(x)\, dx = 0 \tag{67}$$

Similarly, the equilibrium equation for a rigid body displacement of the stringer in the z-direction is

$$\int_{-l}^{l} \lambda_{zs}(x)\, dx = 0 \tag{68}$$

If the ring is considered in its entirety, that is, as made up of an integer number of repeating units around its circumference, the rigid body motions that lead to non-trivial equilibrium conditions are a displacement in the x-direction and a rotation about the x-axis. The x-direction equilibrium equation is

$$\int_{-\Theta}^{\Theta} \lambda_{xr}(\theta)\, (R_0 + e_r)\, d\theta = 0 \tag{69}$$

and the moment equilibrium equation about the x-axis is

$$\int_{-\Theta}^{\Theta} \lambda_{\theta r}(\theta)\, (R_0 + e_r)^2\, d\theta = 0 \tag{70}$$

Equilibrium Eqs. (67) to (69) imply that coefficients

$$\lambda_{xs20} = 0 \qquad \lambda_{zs20} = 0 \qquad \lambda_{xr0} = 0 \tag{71}$$

in the Fourier Series for the interacting loads, and these conditions have been taken into account in Eqs. (61) to (63). The sine series for $\lambda_{\theta r}$ given in Eq. (64) satisfies the equilibrium condition given in Eq. (70).

Consider the variational form of the constraints, Eqs. (46) and (47), for the constant components of the virtual interacting loads. These equations are

$$\Big[u_{200} - \frac{t}{2}\phi_{x200} + \sum_{n=1}^{N}(u_{20n} - \frac{t}{2}\phi_{x20n}) - (u_{s20} + e_s\phi_{\theta s20})\Big]\delta\lambda_{xs20} = 0 \tag{72}$$

$$\Big[\sum_{n=0}^{N} w_{10n} - w_{s20}\Big]\delta\lambda_{zs20} = 0 \tag{73}$$

$$\Big[u_{200} - \frac{t}{2}\phi_{x200} + \sum_{m=1}^{M}(u_{2m0} - \frac{t}{2}\phi_{x2m0}) - (u_{r0} + e_r\phi_{\theta r0})\Big]\delta\lambda_{xr0} = 0 \tag{74}$$

Since these equations are satisfied on the basis that $\delta\lambda_{xs20} = 0$, $\delta\lambda_{zs20} = 0$ and $\delta\lambda_{xr0} = 0$, consistent with Eq. (71), the bracketed terms in Eqs. (72) to (74) do not necessarily vanish. The implication that these bracketed terms in Eqs. (72) to (74) do not vanish is that displacement continuity conditions are not satisfied pointwise. Pointwise continuity can be achieved by taking each Fourier coefficient appearing in the bracketed terms of Eqs. (72) to (74) to be individually zero. Fourier Series given in Eqs. (49), (52), (54), (56), (57), and (60) reflect this choice. Moreover, Fourier coefficients u_{200}, u_{s20}, and u_{r0} represent rigid body displacement in the axial direction for the shell, stringer, and ring, respectively, and setting them to zero can be justified on the basis that rigid body displacement does not contribute to the deformation of the structural elements. Since Fourier coefficient w_{s20} repersents rigid body displacement of the stringer in the z-direction, it would seem that it

should be set to zero as well. However, to maintain continuity between the stringer and the shell in the z-direction, we impose the condition

$$\sum_{n=0}^{N} w_{10n} - w_{s20} \;=\; 0 \tag{75}$$

to determine w_{s20} after obtaining the solution for the displacement components that deform the shell; i.e., Fourier coefficients w_{10n}, $n = 1, ..., N$, are taken to be non-zero independent degrees of freedom since the stringer coefficient w_{s20} is not a part of the solution vector.

Finally, consider the constraint equation associated with $\delta\Lambda_{\theta r0}$, the spatially uniform component of the interacting moment intensity, which was omitted in the series given by Eq. (66). Derived from Eq. (47), this constraint equation is

$$\Big[\sum_{m=1}^{M} \alpha_m w_{2m0} + \phi_{\theta r0}\Big]\delta\Lambda_{\theta r0} \;=\; 0 \tag{76}$$

We equated the constant component of the twist, $\phi_{\theta r0}$, to zero from the considerations associated with Eq. (74). Consequently, a non-zero value of the constant component of the interaction moment intensity, $\Lambda_{\theta r0} \neq 0$, would not contribute to the equilibrium of the ring, since $\Lambda_{\theta r0}$ and $\phi_{\theta r0}$ are conjugate variables in the external work for the ring (refer to Eq. (37)). Since $\phi_{\theta r0} = 0$, it is necessary that $\Lambda_{\theta r0} = 0$ to achieve consistent conditions for the torsional and out-of-plane bending equilibrium of the ring. With $\delta\Lambda_{\theta r0} = 0$ in Eq. (76), the bracketed term does not necessarily vanish, and as a result pointwise rotational continuity betwen the shell and the ring is not assured. Pointwise rotational continuity is achieved if we take the coefficients $w_{2m0} = 0$, $m = 1, ..., M$, as was done in the Fourier Series for the normal displacement of the shell given by Eq. (51).

DISCRETE EQUATIONS AND THEIR SOLUTION

Transverse Shear Deformation Model

The discrete displacement vector for the shell is the $(10MN+3M+3N+2)\times 1$ vector

$$\hat{u}_{shell} = \left[\hat{u}_0^T, \hat{u}_1^T, ..., \hat{u}_M^T\right]^T \tag{77}$$

in which subvectors are

$$\hat{u}_0 = \left[q_0, w_{100}, v_{101}, w_{101}, \phi_{\theta 101}, ..., v_{10N}, w_{10N}, \phi_{\theta 10N}\right]^T \tag{78}$$

$$\begin{aligned}\hat{u}_m = \big[&u_{1m0}, w_{1m0}, \phi_{x1m0}, u_{1m1}, u_{2m1}, v_{1m1}, v_{2m1}, w_{1m1}, w_{2m1}, \phi_{x1m1}, \phi_{x2m1},\\ &\phi_{\theta 1m1}, \phi_{\theta 2m1}, ..., u_{1mN}, u_{2mN}, v_{1mN}, v_{2mN}, w_{1mN}, w_{2mN}, \phi_{x1mN},\\ &\phi_{x2mN}, \phi_{\theta 1mN}, \phi_{\theta 2mN}\big]^T\end{aligned} \tag{79}$$

where $m = 1, ..., M$

The $(6M+1)\times 1$ discrete displacement vector for the stringer and $(4N+1)\times 1$ vector for the ring are

$$\begin{aligned}\hat{u}_{str} = \big[&q_1, u_{s11}, u_{s21}, w_{s11}, w_{s21}, \phi_{\theta s11}, \phi_{\theta s21}, ..., u_{s1M}, u_{s2M},\\ &w_{s1M}, w_{s2M}, \phi_{\theta s1M}, \phi_{\theta s2M}\big]^T\end{aligned} \tag{80}$$

$$\hat{u}_{ring} = \left[w_{r0}, u_{r1}, v_{r1}, w_{r1}, \phi_{\theta r1}, ..., u_{rN}, v_{rN}, w_{rN}, \phi_{\theta rN}\right]^T \tag{81}$$

in which the term w_{s0} for the stringer has been omitted as discussed in reference to Eq. (75). The $4M\times 1$ discrete interacting loads vector for the shell-stringer interface and $(4N+1)\times 1$ vector for the shell-ring interface are

$$\hat{\lambda}_{str} = \left[\lambda_{xs11}, \lambda_{xs21}, \lambda_{zs11}, \lambda_{zs21}, ..., \lambda_{xs1M}, \lambda_{xs2M}, \lambda_{zs1M}, \lambda_{zs2M}\right]^T \tag{82}$$

$$\hat{\lambda}_{ring} = \left[\lambda_{zr0}, \lambda_{xr1}, \lambda_{\theta r1}, \lambda_{zr1}, \Lambda_{\theta r1}, ..., \lambda_{xrN}, \lambda_{\theta rN}, \lambda_{zrN}, \Lambda_{\theta rN}\right]^T \tag{83}$$

Classical Model

The discrete displacement vector for the shell is the $(6MN+2M+2N+2)\times 1$ vector

$$\hat{u}_{shell} = \left[\hat{u}_0^T, \hat{u}_1^T, ..., \hat{u}_M^T\right]^T \tag{84}$$

in which subvectors are

$$\hat{u}_0 = \left[q_0, w_{100}, v_{101}, w_{101}, ..., v_{10N}, w_{10N}\right]^T \tag{85}$$

$$\hat{u}_m = \left[u_{1m0}, w_{1m0}, u_{1m1}, u_{2m1}, v_{1m1}, v_{2m1}, w_{1m1}, w_{2m1}, ..., u_{1mN}, u_{2mN}, v_{1mN}, v_{2mN}, w_{1mN}, w_{2mN}\right]^T \quad \text{where } m = 1, ..., M \tag{86}$$

The $(4M + 1) \times 1$ discrete displacement vector for the stringer and $(4N + 1) \times 1$ vector for the ring are

$$\hat{u}_{str} = \left[q_1, u_{s11}, u_{s21}, w_{s11}, w_{s21}, ..., u_{s1M}, u_{s2M}, w_{s1M}, w_{s2M}\right]^T \tag{87}$$

$$\hat{u}_{ring} = \left[w_{r0}, u_{r1}, v_{r1}, w_{r1}, \phi_{\theta r1}, ..., u_{rN}, v_{rN}, w_{rN}, \phi_{\theta rN}\right]^T \tag{88}$$

The $4M \times 1$ discrete interacting loads vector for the shell-stringer interface and $(4N + 1) \times 1$ vector for the shell-ring interface are the same as for the shear deformation model and are given by Eqs. (82) and (83).

The approximations in Eqs. (49) through (60) for the displacements and Eqs. (61) through (66) for the interacting loads are substituted into the virtual work functionals for each structural element, and also substituted into the variational form of displacement continuity constraints. Then integration over the space is performed. (The test space of virtual displacements and the virtual interacting loads is the same space used for the approximations in Eqs. (49-66).) This process results in a $10MN+13M+11N+6$ system of equations for the transverse shear deformation model and $6MN + 10M + 10N + 6$ system of equations for the classical model, governing the displacements and the interacting loads. The governing equations are of the form

$$\begin{bmatrix} K_{11} & 0 & 0 & B_{11} & B_{12} & B_{13} \\ 0 & K_{22} & 0 & B_{21} & 0 & B_{23} \\ 0 & 0 & K_{33} & 0 & B_{32} & 0 \\ B_{11}^T & B_{21}^T & 0 & 0 & 0 & 0 \\ B_{12}^T & 0 & B_{32}^T & 0 & 0 & 0 \\ B_{13}^T & B_{23}^T & 0 & 0 & 0 & 0 \end{bmatrix} \begin{Bmatrix} \hat{u}_{shell} \\ \hat{u}_{str} \\ \hat{u}_{ring} \\ \hat{\lambda}_{str} \\ \lambda_{ring} \\ Q \end{Bmatrix} = \begin{Bmatrix} F_{11} \\ 0 \\ 0 \\ 0 \\ 0 \\ 0 \end{Bmatrix} \tag{89}$$

in which sub-matrices K_{11}, K_{22} and K_{33} are the stiffness matrices for the shell, stringer, and ring, respectively. The sub-matrices $B_{ij}, i, j = 1, 2, 3$, in Eq. (89) are determined from the external virtual work terms involving the interacting loads, and the constraint Eqs. (46) to (48). The vector on the right-hand-side of Eq. (89) is the force vector, determined from the external virtual work terms involving pressure. The constraint equations correspond to the last three rows of the partitioned matrix in Eq. (89). Equation (89) is first solved for the displacements in terms of interacting loads, then this solution is substituted into the constraint equations to determine the interacting loads. Thus, the total solution is obtained.

NUMERICAL EXAMPLE

Numerical data for the example are $R = 117.5$ in., $2l = 20$ in. and $2R\Theta = 5.8$ in., which is typical of a large transport aircraft. The shell wall is a 16-ply quasi-isotropic $[\pm 45, 0, 90, \pm 45, 0, 90]_s$ laminate of graphite/epoxy tape with a total thickness of 0.080 in. The ply thickness is 0.005 in., and the lamina material properties are $E_1 = 1.85 \times 10^7 lb/in.^2$, $E_2 = 1.64 \times 10^6 lb/in.^2$, $G_{12} = G_{13} = 0.87 \times 10^6 lb/in.^2$, $G_{23} = 0.49 \times 10^6 lb/in.^2$, and $\nu_{12} = 0.3$. For the transverse shear deformation model, the shell wall stiffness sub-matrices of Eq. (23) are computed using these ply data and the expressions for the stiffness elements given in the Appendix. The numerical results are

$$A = \begin{bmatrix} 0.654 & 0.198 & 0 \\ 0.198 & 0.654 & 0 \\ 0 & 0 & 0.228 \end{bmatrix} \times 10^6 \ lb/in.$$

$$B = \begin{bmatrix} 2.915 & 0 & 0.0904 & 0.0904 \\ 0 & -2.481 & -0.0904 & 0.0904 \\ 0 & -0.181 & -0.652 & 0.652 \end{bmatrix} lb$$

$$D = \begin{bmatrix} 342.52 & 137.25 & 0 & 0 \\ 137.25 & 291.53 & 0 & -0.14 \times 10^{-5} \\ 0 & 0 & 153.21 & -0.30 \times 10^{-5} \\ 0 & -0.14 \times 10^{-5} & -0.30 \times 10^{-5} & 0.30 \times 10^{-5} \end{bmatrix} lb\ in.$$

and A_{ij} elements for the transverse shear stiffness matrix of Eq.(24) are

$$A_{44} = A_{55} = 0.544 \times 10^5 \ lb/in., \qquad A_{45} = 0$$

The bending and stretching-bending coupling sub-matrices for classical lamination theory, Eq. (35), are given by

$$D = \begin{bmatrix} 342.52 & 137.25 & 0 \\ 137.25 & 291.53 & 0 \\ 0 & 0 & 153.21 \end{bmatrix} lb\ in. \qquad B = 0$$

The extensional stiffness sub-matrix A is the same for classical theory and shear deformation theory. Numerical data for the stiffeners are shown in Fig. 4. All the results presented are for an internal pressure $p = 10$ psi, and the Fourier Series are truncated at twenty-four terms in the x- and θ-directions ($M = N = 24$).

RESULTS AND DISCUSSION

Interacting Load Distributions

The distributions of the interacting loads between the stringer and the shell are shown in Figs. 5 and 6. The distributions of the tangential component, λ_{xs}, shown in Fig. 5 are asymmetric about the origin (or stiffener intersection), and the maximum value in the transverse shear deformation theory is less by about 40% with respect to the maximum value in the classical theory. The distributions of the normal component, λ_{zs}, are also asymmetric about the origin (Fig. 6). The peak value of normal component computed from the classical model is 920.2 lb/in. and occurs at $x = 0.2$ inches. The peak value of normal component computed from the shear deformation model is 669.3 lb/in. and occurs at the origin. That is, the peak value of λ_{zs} is reduced by 27% in the transverse shear deformation model with respect to its peak value in the classical model. It is interesting to note that the asymmetric response predicted by the classical model is more predominant compared to the transverse shear deformation model.

The distributions of the interacting loads between the ring and the shell are shown in Figs. 7 through 10. The distributions of axial force intensity, λ_{xr}, are symmetric about the origin, and attain extremum values at the origin as shown in Fig. 7. The extremum value of the axial force component is reduced from -144.3

lb/in. in the classical model to -20.3 lb/in. in the transverse shear deformation model (an 86% reduction). As shown in Fig. 8, the distributions of the tangential force component, $\lambda_{\theta r}$, are antisymmetric about the origin, and the differences in the results for $\lambda_{\theta r}$ from the two models are small. The distributions of the normal force intensity, λ_{zr}, are symmetric about the origin as shown in Fig. 9 and the predictions obtained from the two models are essentially the same. The normal force intensity is an extremum at the origin attaining a value of -2316.9 lb/in. in this example. The distributions of tangential moment component, $\Lambda_{\theta r}$, are symmetric about the origin, and attain extremum values at the origin as shown in Fig. 10. The maximum value of the tangential moment component is reduced from 525.2 lb-in./in. in the classical model to 30.5 lb-in./in. in the transverse shear deformation model (a 94% reduction). Results for λ_{xr} and $\Lambda_{\theta r}$ shown in Figs. 7 and 10, respectively, indicate that classical theory exaggerates the response of these variables, which are particularly sensitive to the asymmetry introduced by the ring.

Stiffener Actions

The distributions of the force and moment resultants in the stiffeners are shown in Figs. 11 through 13. The stringer axial force and bending moment distributions (Fig. 11) are slightly asymmetric about the origin, and only small differences are predicted between the two models.

The distributions of the circumferential force and in-plane bending moment in the ring are shown in Fig. 12, and, again, there are only small differences in these results from the two models. However, the torque and out-of-plane bending moment in the ring are more sensitive to the change in models as shown Fig. 13. The distribution of the out-of-plane bending moment is symmetric about the origin and has reduced magnitudes in the transverse shear deformation model compared to the classical model. In the vicinity of origin, the transverse shear deformation model predicts less severe gradients in the distribution of out-of-plane bending moment compared to the classical model. As shown in Fig. 13, the distribution of torsion

is antisymmetric about the origin, and has reduced magnitudes in classical model compared to the shear deformation model.

Shell Response

The distribution of the normal displacement along x-curve midway between the stringers ($\theta = -\Theta$), and along the θ-curve midway between the rings ($x = -l$), are shown in Fig. 14. As depicted in this figure, there is a negligible difference between the results from the transverse shear deformation model and classical model. Also, there is negligible difference in the axial and circumferential normal strain distributions between the two models as shown in Figs. 15 and 16.

A Ring with Symmetric Cross Section

As a benchmark for comparing transverse shear deformation model with the classical model, analyses were performed for a ring with symmetric cross section. In this case the only change made to the example under discussion is to set the bending-coupling stiffeness EI_{zx} of the ring to zero from its value given in Fig. 4. Consequently, the θ-axis, as well as the x-axis, are axes of symmetry for the repeating unit. Symmetry about the θ-axis implies there is no out-of-plane bending and torsion of the ring; i.e., $u_r(\theta) = \phi_{\theta r}(\theta) = \phi_{zr}(\theta) = \lambda_{xr}(\theta) = \Lambda_{\theta r}(\theta) = 0$ for $-\Theta \leq \theta \leq \Theta$.

The distributions of the tangential interacting loads between the shell and the stiffeners are shown in Figs. 17 and 18. For the tangential force intensity between the stringer and shell (Fig. 17), the difference between the results from the transverse shear deformation model and classical model are small. For tangential force intensity between the ring and shell (Fig. 18), the differences in the results from the two models are larger than those for the stringer-shell tangential force intensity. However, differences between the two models for the ring-shell tangential force intensity are not excessively large. The tangential force intensity components between the stiffeners and shell are the most sensitive variables to a change in structural model. All other dependent variables are only affected by negligible amounts to the change in structural models.

CONCLUSIONS

The results for the shell-stringer interacting loads λ_{xs} and λ_{zs}, and shell-ring interacting loads λ_{xr} and $\Lambda_{\theta r}$, indicate that the classical structural model exaggerates the asymmetric response compared to the transverse shear deformation model. The predicted extremum values of these interacting load components are smaller in the transverse shear deformation theory than in the classical theory. The large discrepancy is due to the freedom in the transverse shear deformation model between the stringer's bending rotation and the ring's torsional rotation at the stiffener intersection, or joint. In the classical model these joint rotations are constrained to be the same. Shell strains and displacements are not significantly different in the two structural models.

ACKNOWLEDGMENT

This research is supported by NASA Grant NAG-1-537, and Dr. James H. Starnes, Jr., NASA Langley Research Center is the technical monitor.

REFERENCES

Jackson, A. C., Campion, M. C., and Pei, G. (1984). Study of utilization of advanced composites in fuselage structures of large transports. *NASA Contractor Report 172404*, Contract NAS1-17415, September.

Johnson, E. R., and Rastogi, N. (1994). Interacting loads in an orthogonally stiffened composite cylindrical shell. *Proceedings of the AIAA/ASME/ASCE/AHS/ASC 35th Structures, Structural Dynamics and Materials Conference* (Hilton Head SC), Part 5, AIAA, Washington, D.C., April, pp. 2607-2620.

Jones, R. M. (1975). *Mechanics of Composite Materials*, Scripta Book Co., Washington DC, pp. 51, 154, 155.

Novozhilov, V. V. (1964). *Thin Shell Theory*, Noordhoff Ltd., The Netherlands, p. 23.

Sanders, J. L. (1959). An improved first approximation theory for thin shells. *NASA Technical Report R-24*, June.

Appendix

ELEMENTS OF STIFFNESS MATRIX FOR A CYLINDRICAL SHELL BASED ON TRANSVERSE SHEAR DEFORMATION THEORY

Based on the transverse shear deformation theory, the elements A_{ij}, B_{ij}, and D_{ij} of the stiffness matrices, in Eqs. (23) and (24) for the constitutive law for a laminated shell wall, are given by

$$A_{11} = \int_t \bar{Q}_{11}(1+\frac{z}{R})dz$$

$$A_{12} = \int_t \bar{Q}_{12}dz$$

$$A_{16} = \int_t \bar{Q}_{16}dz$$

$$A_{22} = \int_t \bar{Q}_{22}(1+\frac{z}{R})^{-1}dz$$

$$A_{26} = \int_t \bar{Q}_{26}(1+\frac{z}{R})^{-1}dz$$

$$A_{66} = \int_t \bar{Q}_{66}(1+\frac{z}{R})^{-1}dz$$

$$B_{11} = \int_t \bar{Q}_{11}z(1+\frac{z}{R})dz$$

$$B_{12} = \int_t \bar{Q}_{12}zdz$$

$$B^1_{16} = \int_t \bar{Q}_{16}z(1+\frac{z}{R})dz$$

$$B^2_{16} = \int_t \bar{Q}_{16}\frac{z^2}{2R}dz$$

$$B_{22} = \int_t \bar{Q}_{22}z(1+\frac{z}{R})^{-1}dz$$

$$B^1_{26} = \int_t \bar{Q}_{26}z(1+\frac{z}{2R})(1+\frac{z}{R})^{-1}dz$$

$$B^2_{26} = \int_t \bar{Q}_{26}\frac{z^2}{2R}(1+\frac{z}{R})^{-1}dz$$

$$B_{61} = \int_t \bar{Q}_{16}zdz$$

$$B_{62} = \int_t \bar{Q}_{16}z(1+\frac{z}{R})^{-1}dz$$

$$B_{66}^{1} = \int_t \bar{Q}_{66} z (1 + \frac{z}{2R})(1 + \frac{z}{R})^{-1} dz$$

$$B_{66}^{2} = \int_t \bar{Q}_{66} \frac{z^2}{2R} (1 + \frac{z}{R})^{-1} dz$$

$$D_{11} = \int_t \bar{Q}_{11} z^2 (1 + \frac{z}{R}) dz$$

$$D_{12} = \int_t \bar{Q}_{12} z^2 dz$$

$$D_{16}^{1} = \int_t \bar{Q}_{16} z^2 (1 + \frac{z}{R}) dz$$

$$D_{16}^{2} = \int_t \bar{Q}_{16} \frac{z^3}{2R} dz$$

$$D_{22} = \int_t \bar{Q}_{22} z^2 (1 + \frac{z}{R})^{-1} dz$$

$$D_{26}^{1} = \int_t \bar{Q}_{26} z^2 (1 + \frac{z}{2R})(1 + \frac{z}{R})^{-1} dz$$

$$D_{26}^{2} = \int_t \bar{Q}_{26} \frac{z^3}{2R} (1 + \frac{z}{R})^{-1} dz$$

$$D_{66}^{11} = \int_t \bar{Q}_{66} z^2 (1 + \frac{z}{2R})^{2} (1 + \frac{z}{R})^{-1} dz$$

$$D_{66}^{12} = \int_t \bar{Q}_{66} \frac{z^3}{2R} (1 + \frac{z}{2R})(1 + \frac{z}{R})^{-1} dz$$

$$D_{66}^{22} = \int_t \bar{Q}_{66} \frac{z^4}{4R^2} (1 + \frac{z}{R})^{-1} dz$$

where $\bar{Q}_{ij}$ are the transformed reduced stiffnesses given in the text by Jones (1975).

Based on the assumption of constant transverse shear strain distribution through the thickness, the transverse shear stiffnesses are given by

$$A_{44} = \int_t C_{44} (1 + \frac{z}{R}) dz$$

$$A_{45} = \int_t C_{45} dz$$

$$A_{55} = \int_t C_{55} (1 + \frac{z}{R})^{-1} dz$$

where

$$C_{44} = G_{13} Cos^2 \alpha + G_{23} Sin^2 \alpha$$

$$C_{45} = (G_{13} - G_{23}) Cos\alpha Sin\alpha$$

$$C_{55} = G_{23} Cos^2\alpha + G_{13} Sin^2\alpha$$

in which α is the ply orientation angle.

Based on the assumption of constant transverse shear stress distribution through the thickness, the transverse shear stiffnesses are given by

$$A_{44} = \frac{k_{22}}{k} \qquad A_{45} = -\frac{k_{12}}{k} \qquad A_{55} = \frac{k_{11}}{k}$$

in which $k = k_{11}k_{22} - k_{12}^2$. The coefficients k_{ij} are given by

$$k_{11} = \frac{1}{t^2} \int_t c_{44} (1 + \frac{z}{R})^{-1} dz$$

$$k_{12} = \frac{1}{t^2} \int_t c_{45} dz$$

$$k_{22} = \frac{1}{t^2} \int_t c_{55} (1 + \frac{z}{R}) dz$$

where

$$c_{44} = \frac{Cos^2\alpha}{G_{13}} + \frac{Sin^2\alpha}{G_{23}}$$

$$c_{45} = (\frac{1}{G_{13}} - \frac{1}{G_{23}}) Cos\alpha Sin\alpha$$

$$c_{55} = \frac{Sin^2\alpha}{G_{13}} + \frac{Cos^2\alpha}{G_{23}}$$

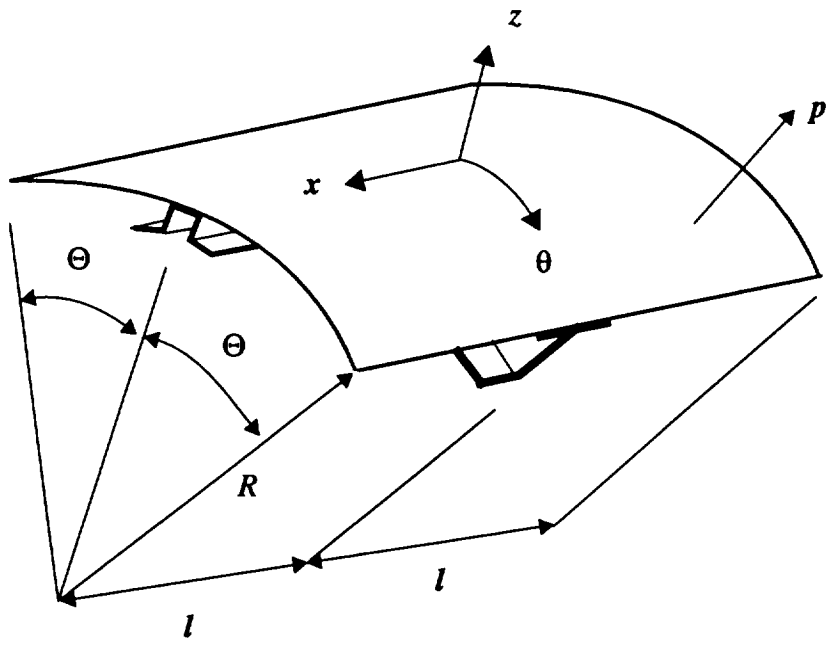

Fig. 1. Repeating unit of an orthogonally stiffened cylindrical shell.

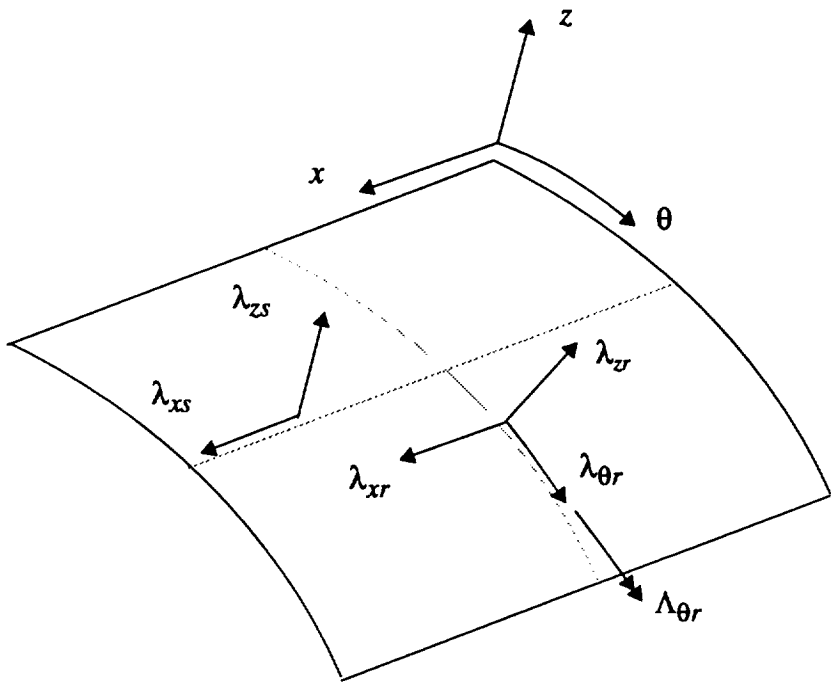

Fig. 2. Interacting line load intensities shown in the positive sense acting on the inside surface of the shell.

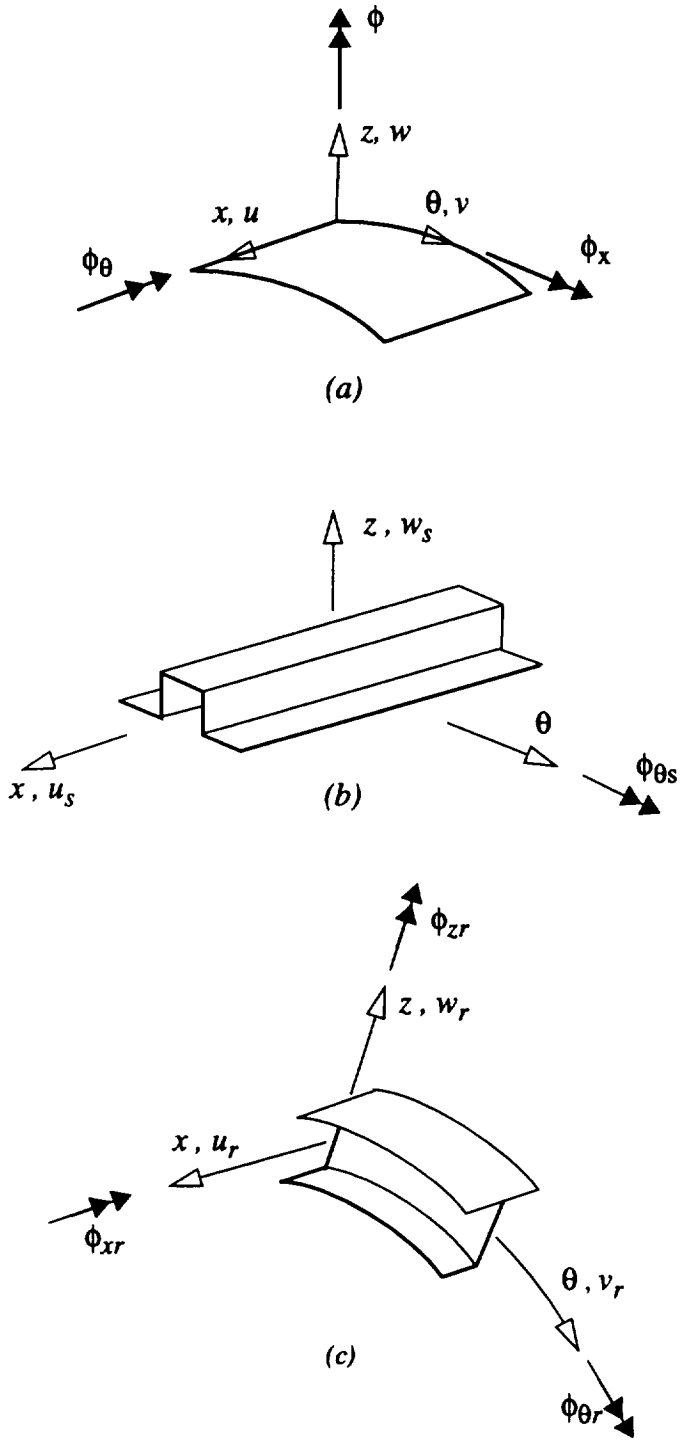

Fig. 3. Displacements and rotations for (a) shell, (b) stringer, and (c) ring

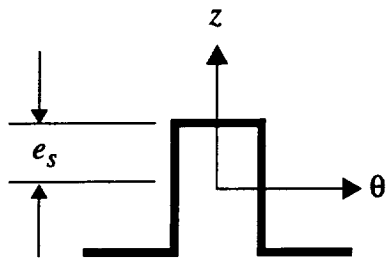

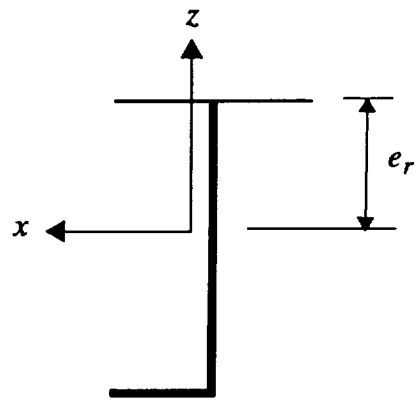

Stringer
$EA = 4.04 \times 10^6$ lb
$EI_{\theta\theta} = 14.2 \times 10^6$ lb-in.^{2}
$(GA)_{xz} = 1.23 \times 10^6$ lb
$e_s = 1.10$ in.

Ring
$EA = 5.92 \times 10^6$ lb
$EI_{xx} = 26.9 \times 10^6$ lb-in.^{2}
$EI_{zz} = 2.69 \times 10^6$ lb-in.^{2}
$EI_{xz} = -8.29 \times 10^6$ lb-in.^{2}
$GJ = 1.0 \times 10^6$ lb-in.^{2}
$e_r = 3.78$ in.

Fig. 4. Stiffener data.

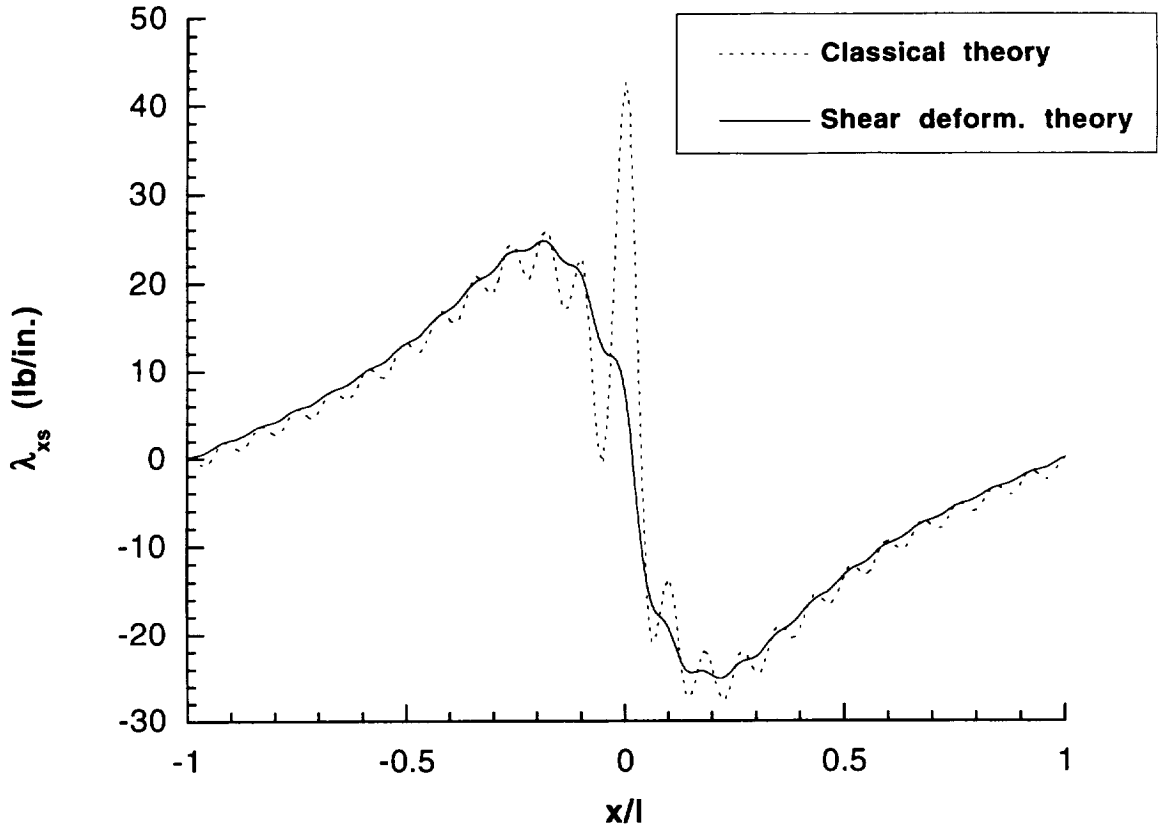

Fig. 5 Stringer-shell tangential force intensity.

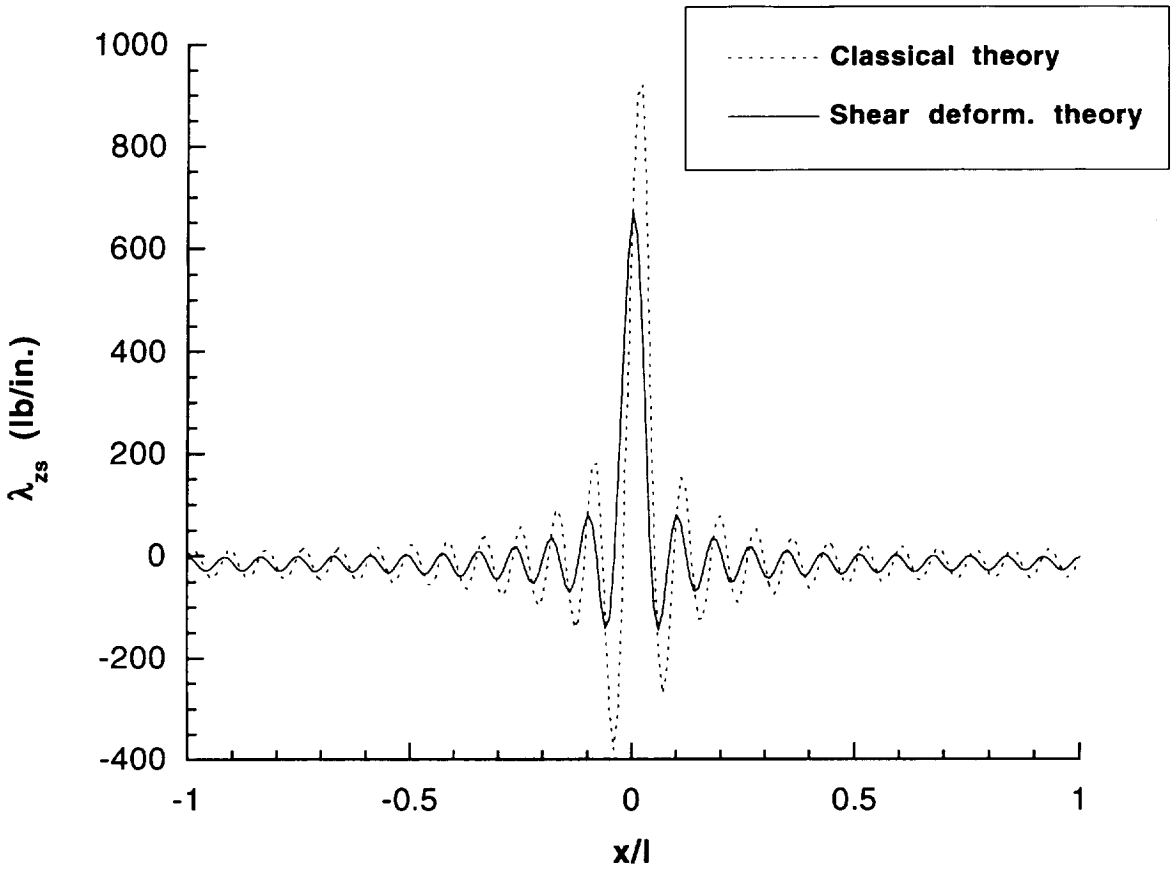

Fig. 6 Stringer-shell normal force intensity.

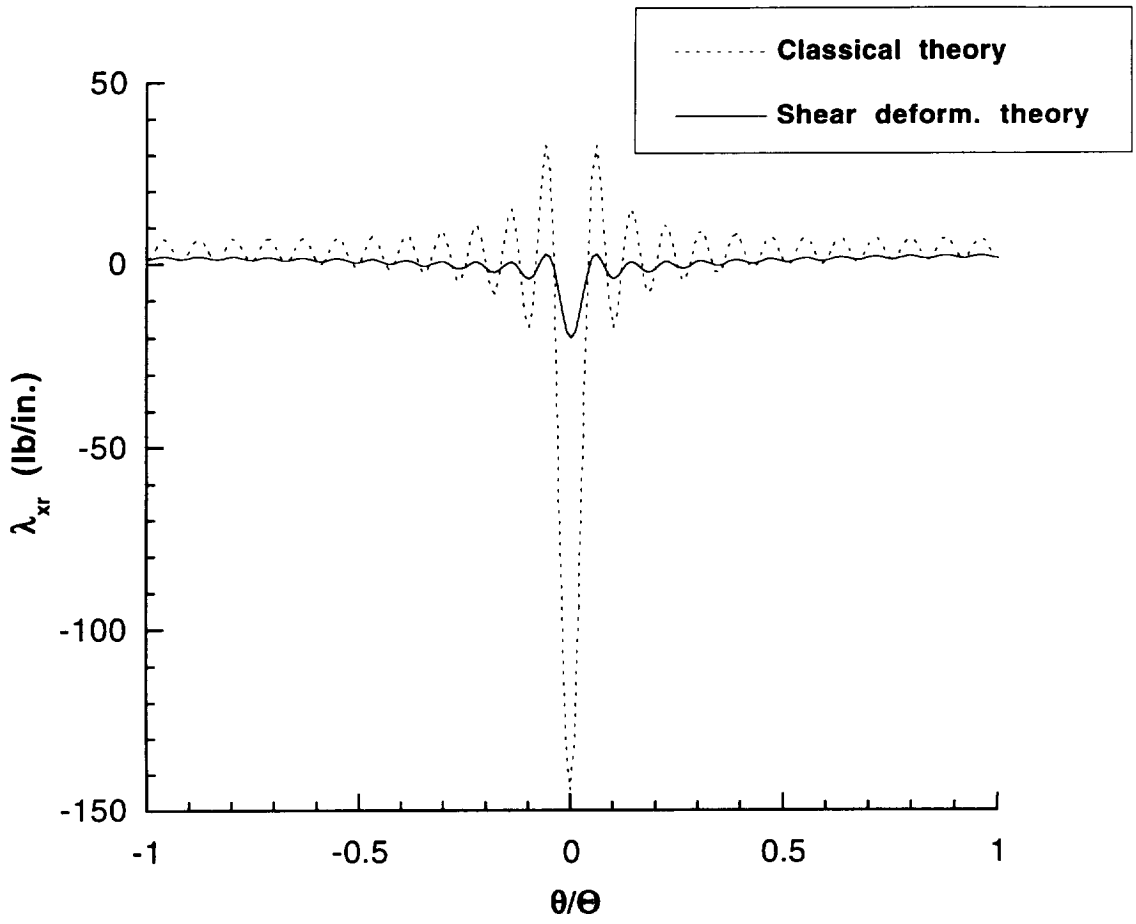

Fig. 7 Ring-shell axial force intensity.

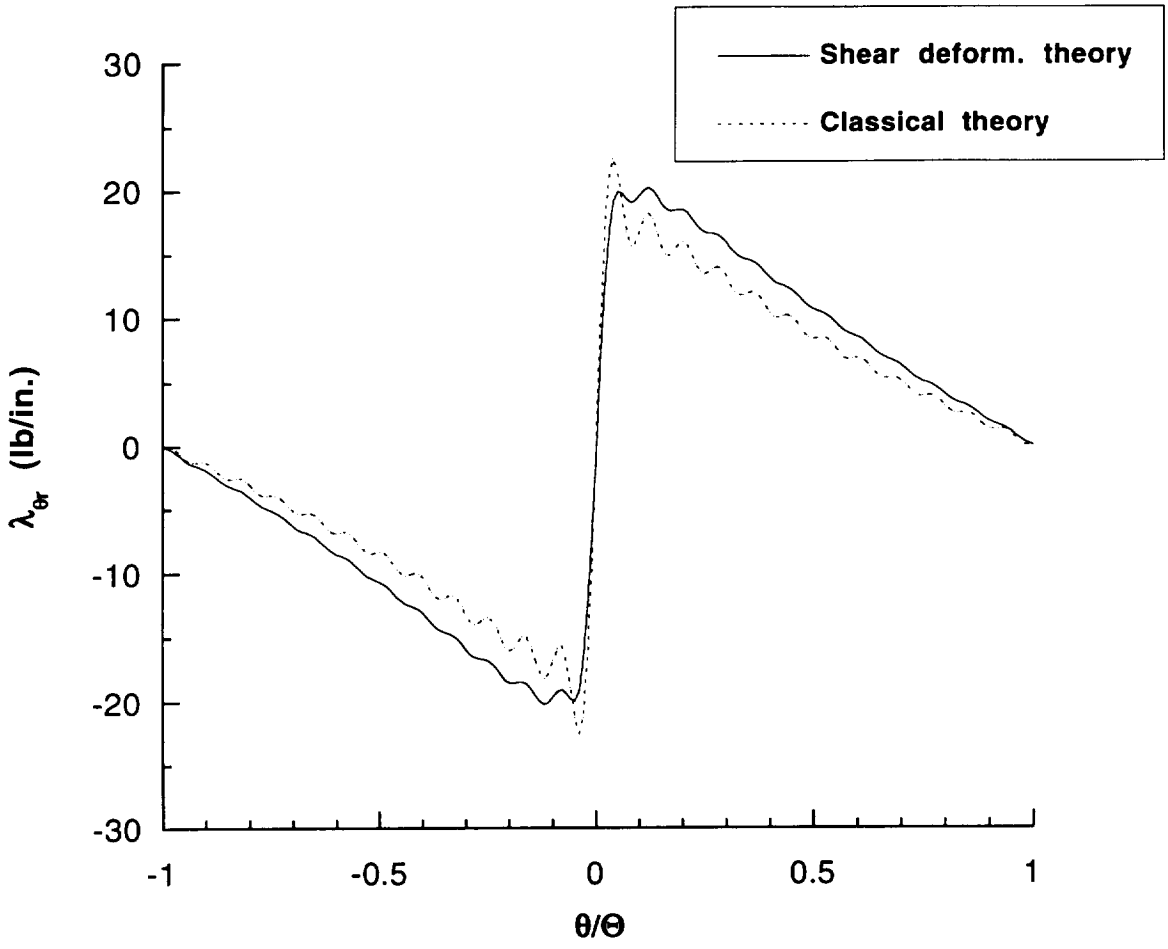

Fig. 8 Ring-shell tangential force intensity.

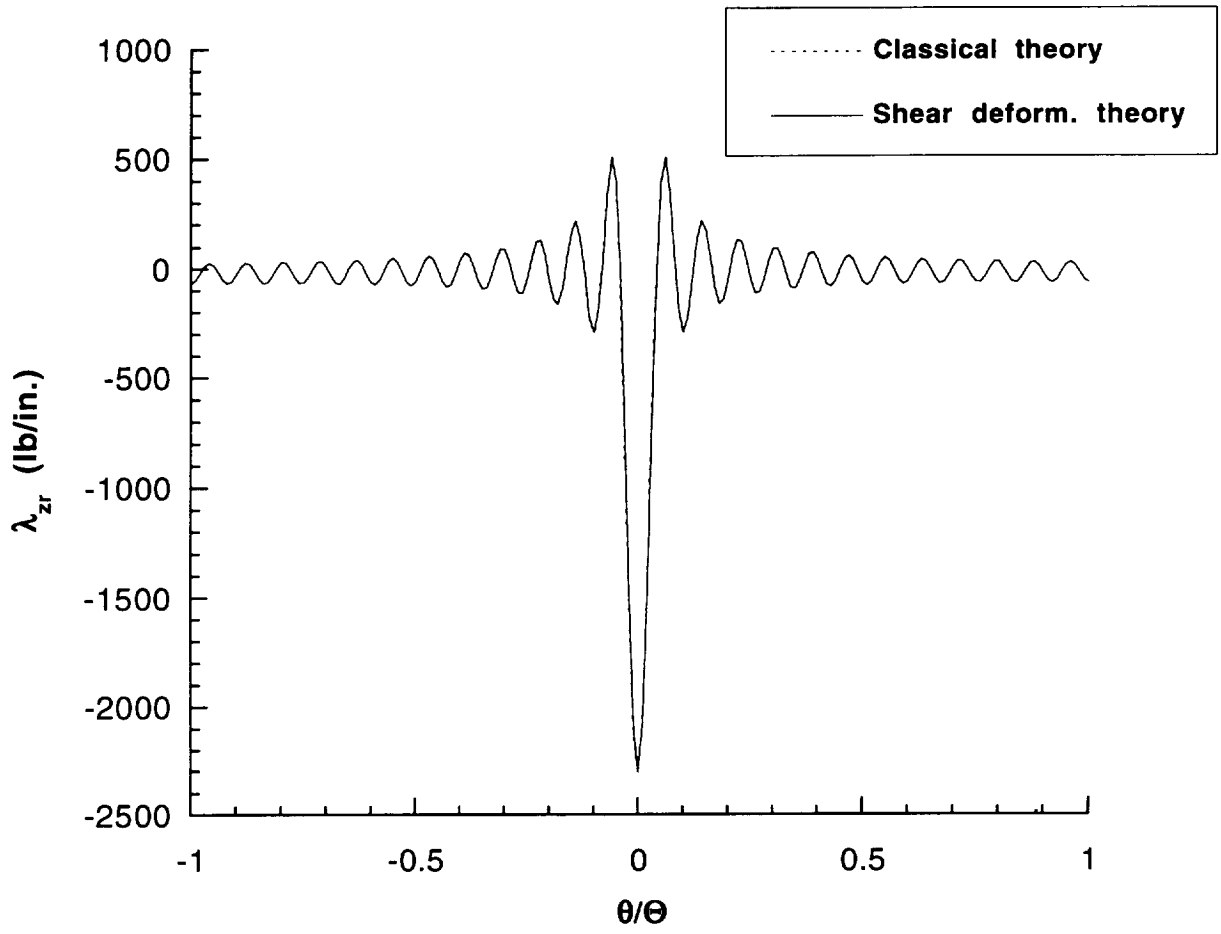

Fig. 9 Ring-shell normal force intensity.

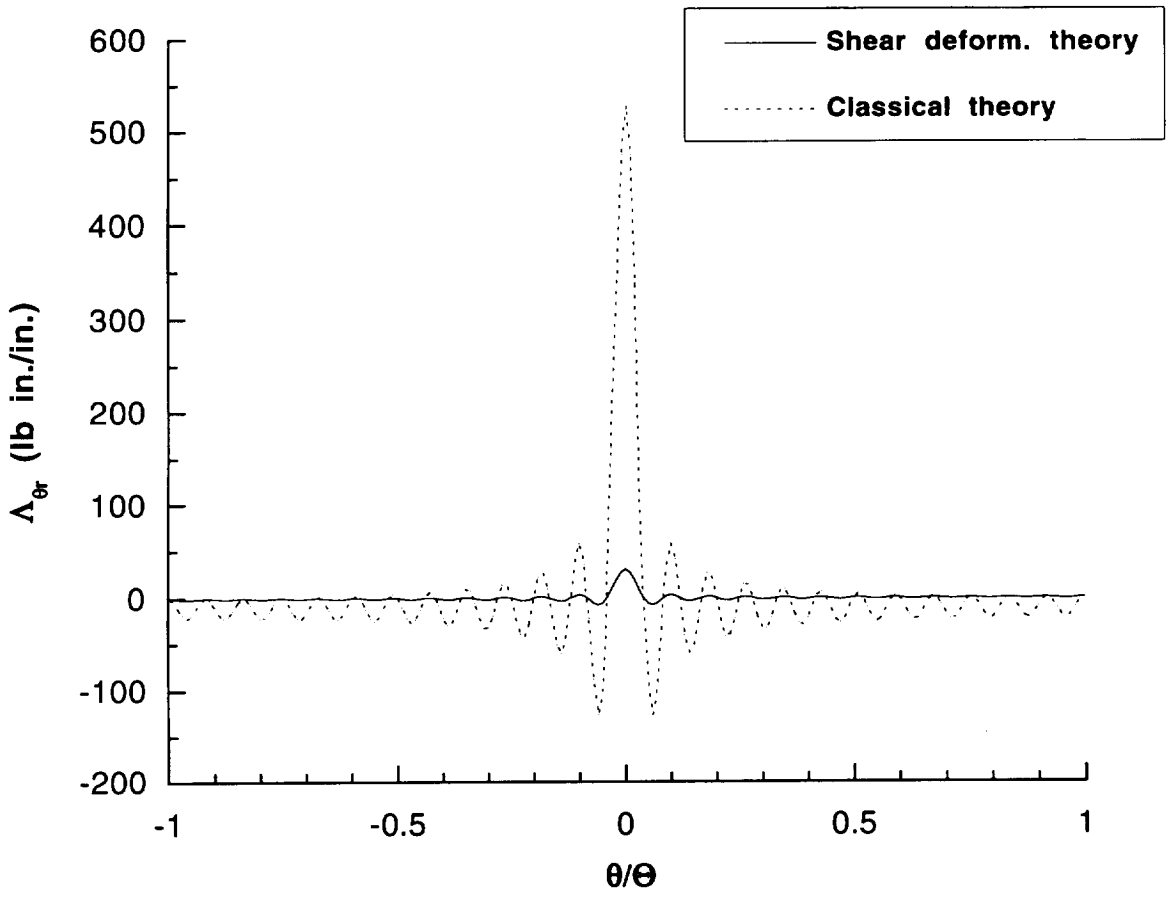

Fig. 10 Ring-shell tangential moment intensity.

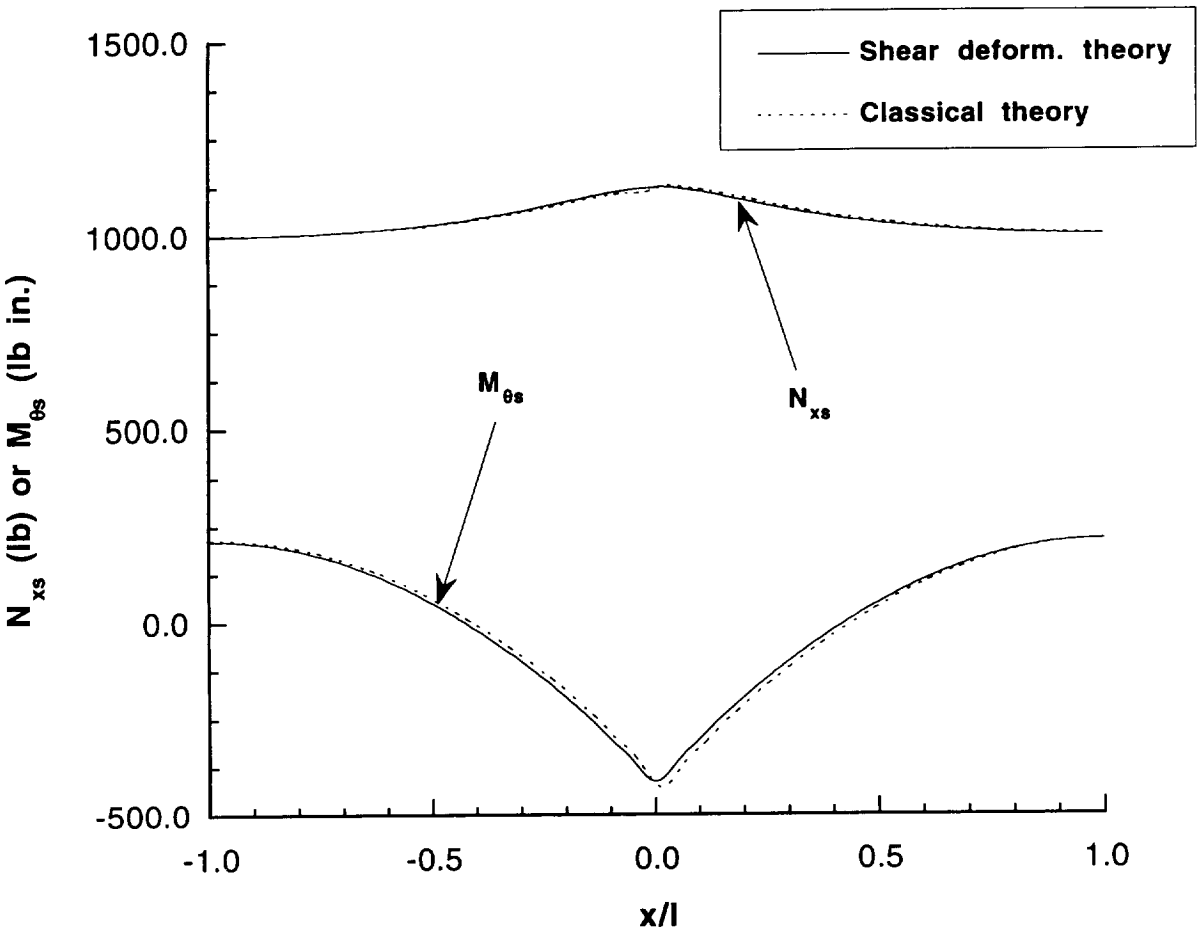

Fig. 11 Stringer axial force and bending moment distribution.

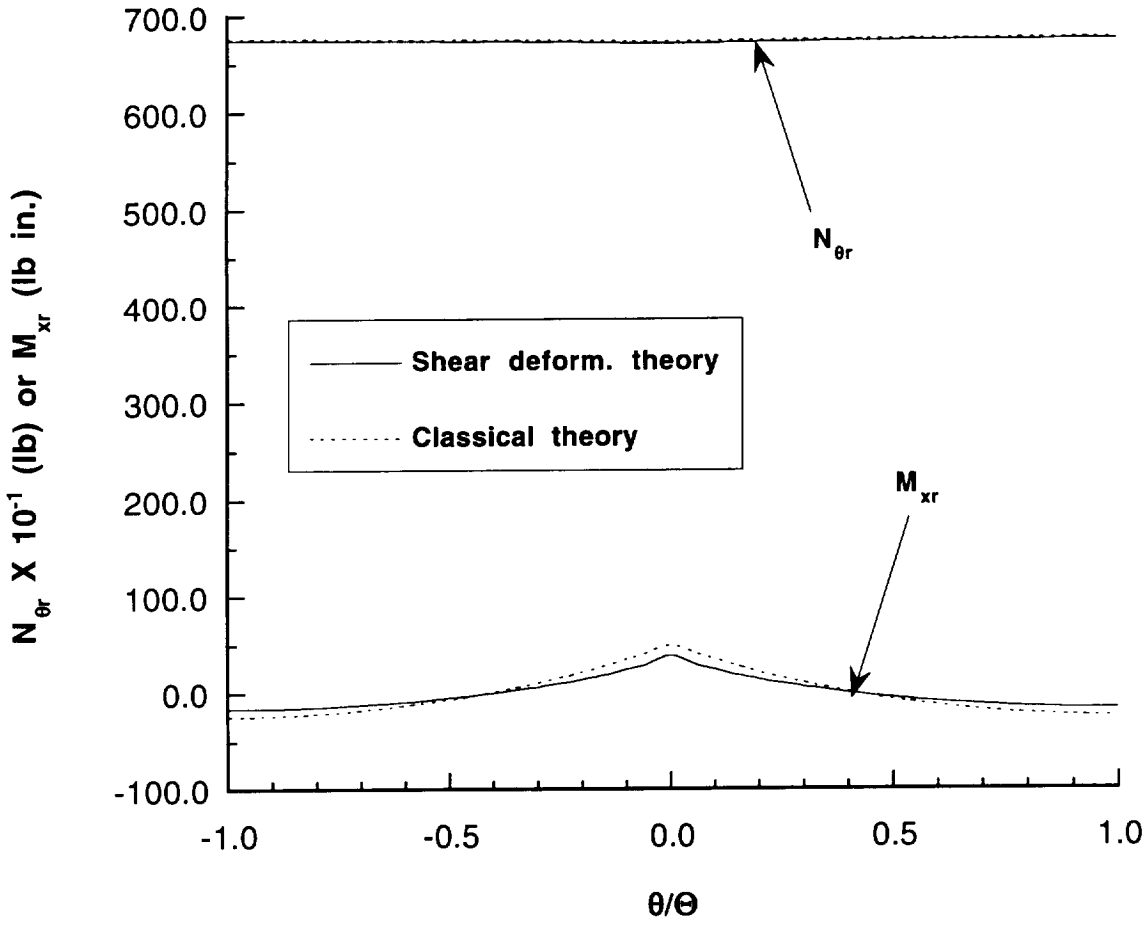

Fig. 12 Ring circumferential force and in-plane bending moment distribution.

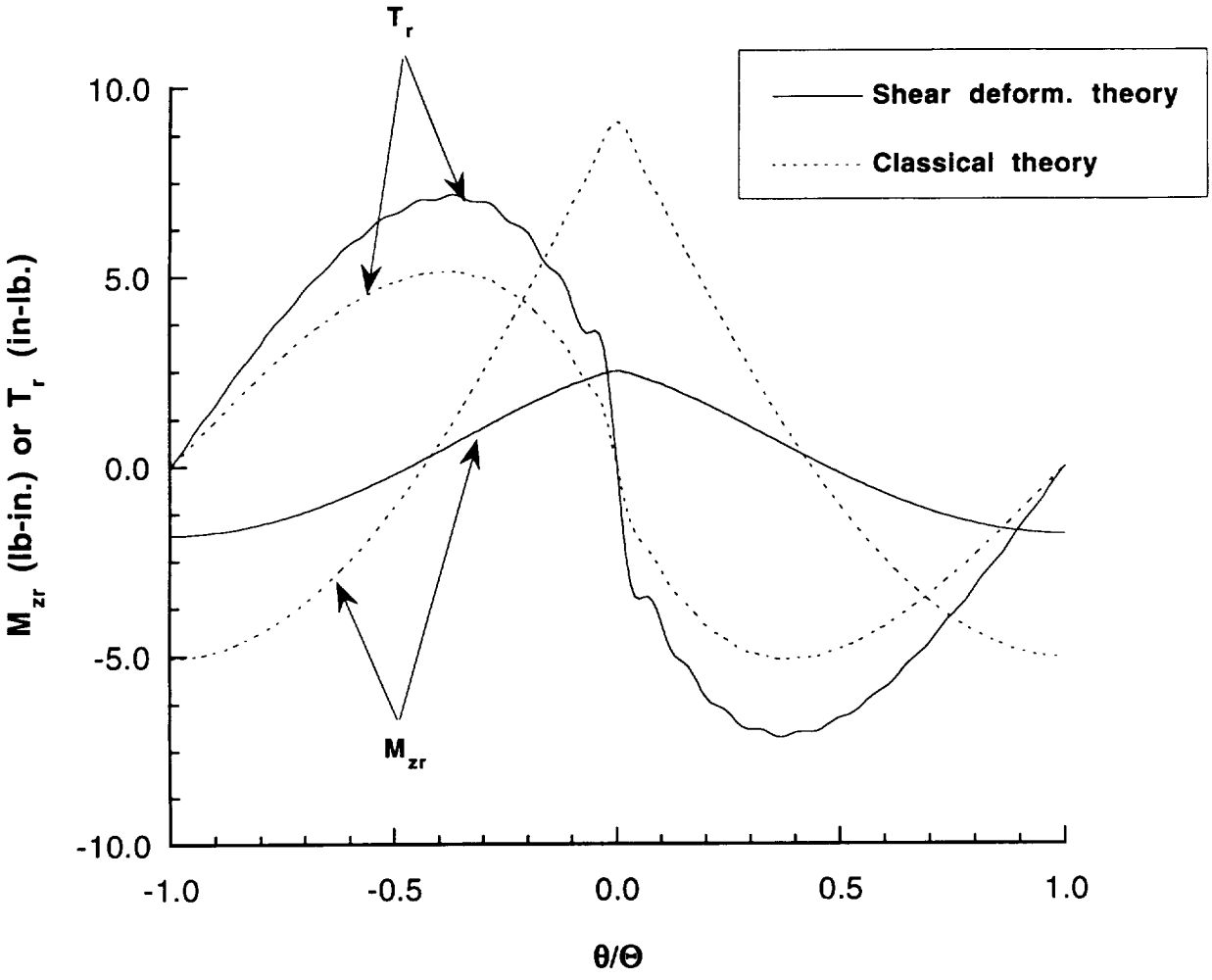

Fig. 13 Ring out-of-plane bending moment and torque distribution.

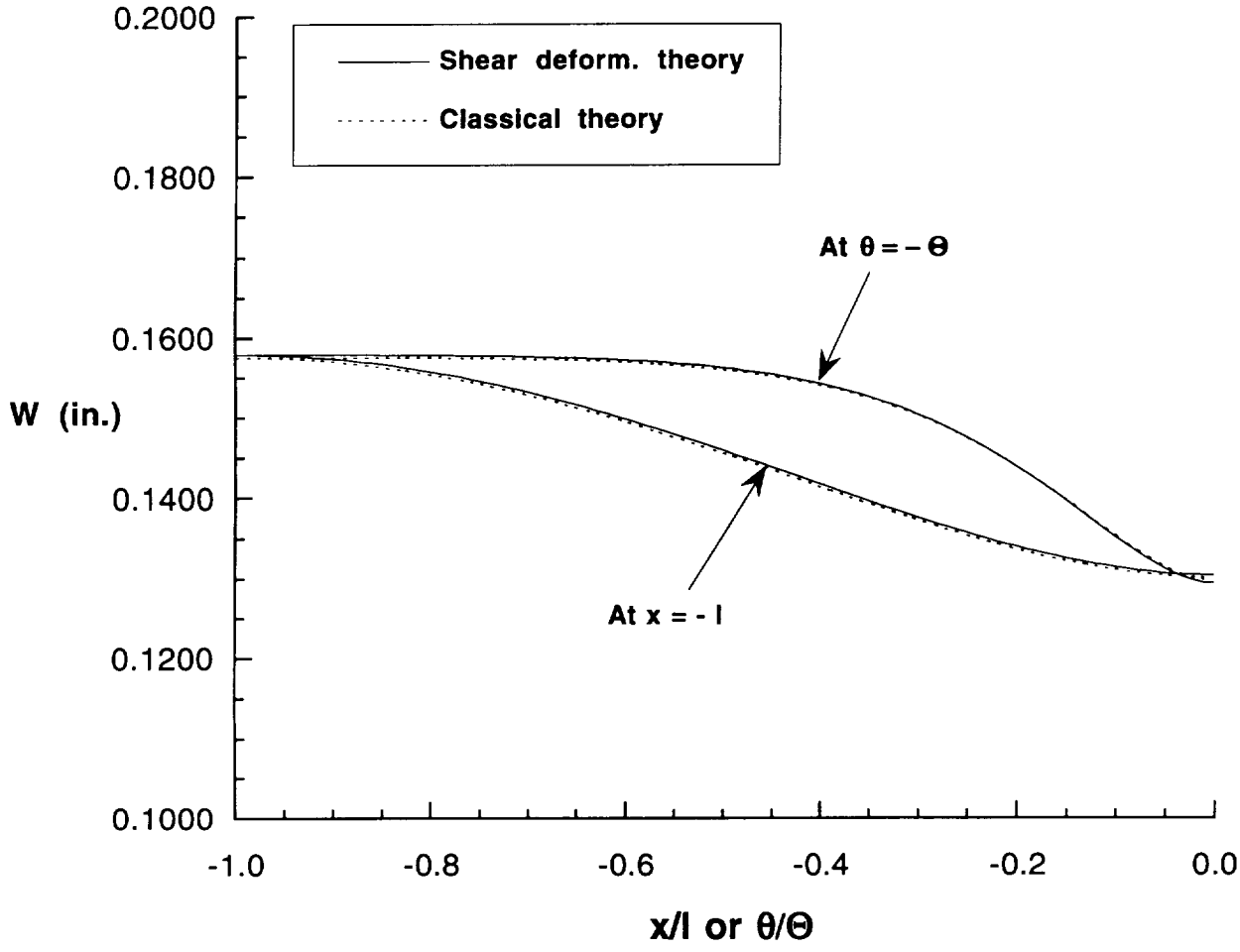

Fig. 14 Distribution of shell's normal displacement.

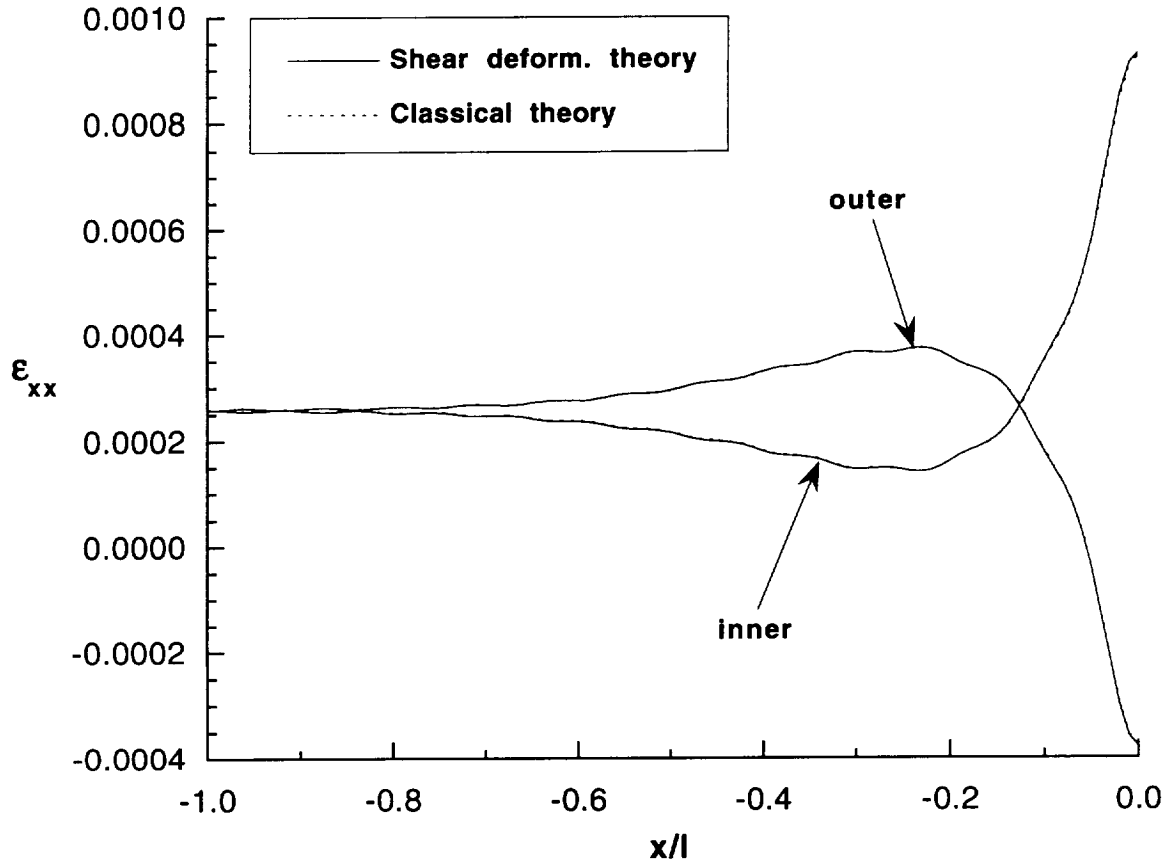

Fig. 15 Distributions of the axial normal strain on the inner and outer shell surfaces midway between the stringers ($\theta = -\Theta$).

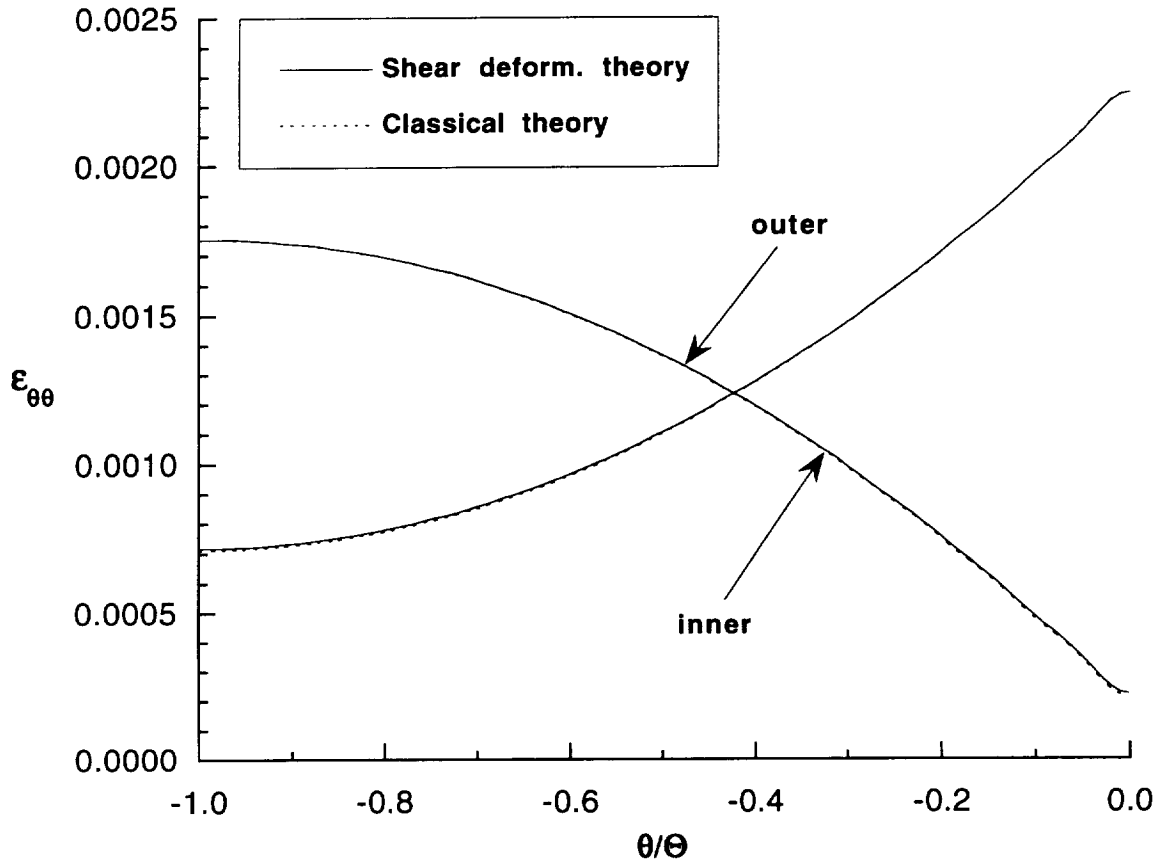

Fig. 16 Distributions of the circumferential normal strain on the inner and outer shell surfaces midway between the rings (x = - l).

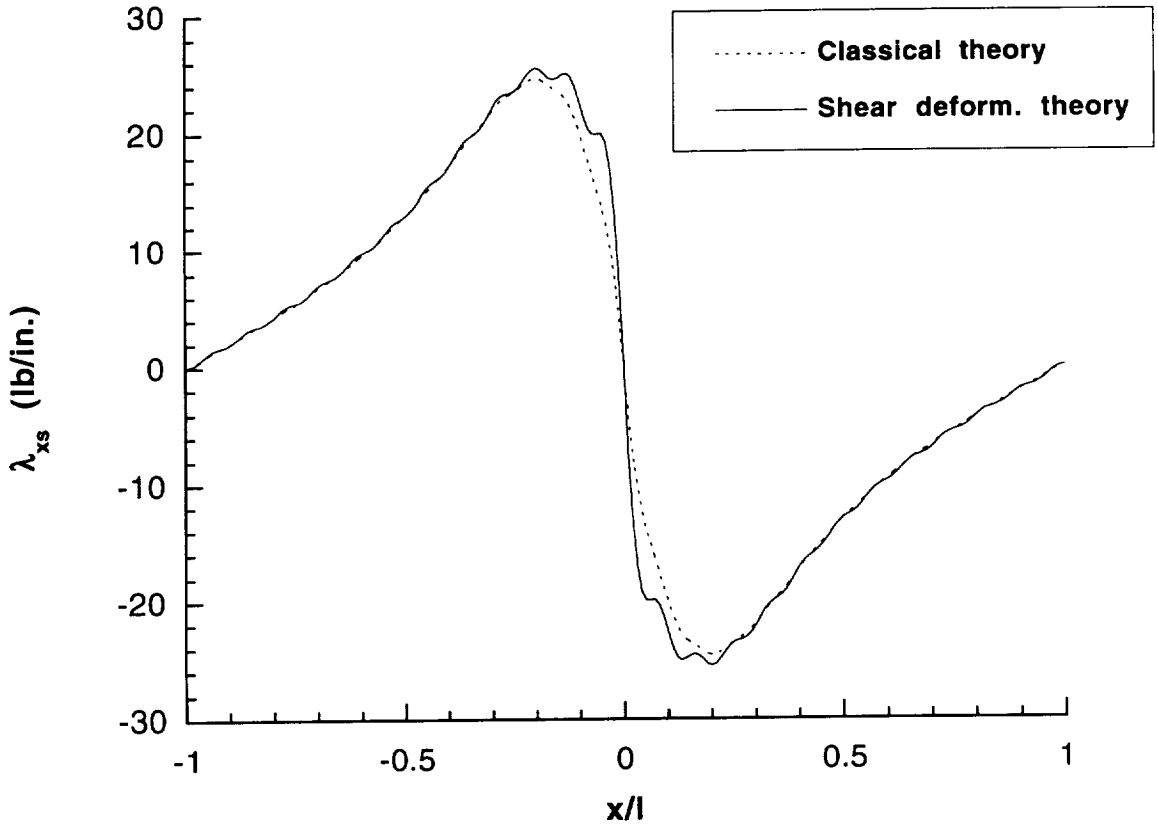

Fig. 17 Stringer-shell tangential force intensity for a ring with symmetrical cross section.

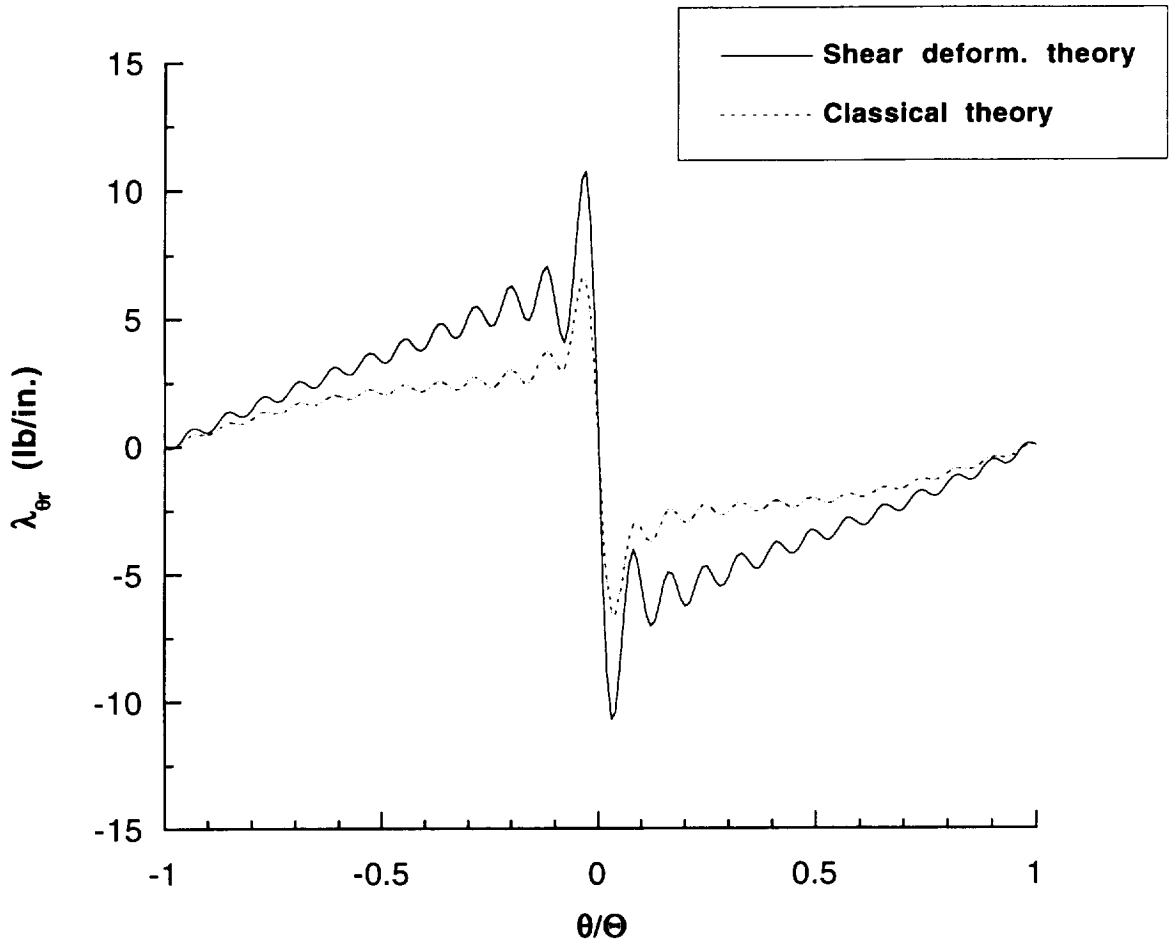

Fig. 18 Ring-shell tangential force intensity for a ring with symmetrical cross section.